Journal of Chromatography A

Robust mechanistic modeling of protein ion-exchange chromatography using a colloidal isotherm

--Manuscript Draft--

Manuscript Number:	
Article Type:	Full length article
Keywords:	mechanistic modeling; protein ion-exchange chromatography; monoclonal antibody; breakthrough curve; parameter estimation
Corresponding Author:	Abraham Lenhoff University of Delaware Newark, DE United States
First Author:	Vijesh Kumar
Order of Authors:	Vijesh Kumar
	Samuel Leweke
	William Heymann
	Eric von Lieres
	Fabrice Schlegel
	Karin Westerberg
	Abraham Lenhoff
Abstract:	Mechanistic models for ion-exchange chromatography of proteins are well-established and a broad consensus exists on most aspects of the detailed mathematical and physical description. A variety of specializations of these models can typically capture the general locations of elution peaks, but discrepancies are often observed in peak position and shape, especially if the column load level is in the non-linear range. These discrepancies may prevent the use of models for high-fidelity predictive applications such as process characterization and development of high-purity and -productivity process steps. Our objective is to develop a sufficiently robust mechanistic framework to make both conventional and anomalous phenomena more readily predictable using model parameters that can be evaluated based on independent measurements or well-accepted correlations. This work demonstrates the implementation of this approach for industry-relevant case studies using both a model protein, lysozyme, and biopharmaceutical product monoclonal antibodies, using cation-exchange resins with a variety of architectures (SP Sepharose FF, Fractogel EMD SO3-, Capto S and Toyopearl SP650M). The modeling employs the general rate model with the extension of the surface diffusivity to be variable, as a function of ionic strength or binding affinity. A colloidal isotherm that accounts for protein-surface and protein-protein interactions independently was used, with each characterized by a parameter determined as a function of ionic strength and pH. Both of these isotherm parameters, along with the variable surface diffusivity, were successfully estimated using breakthrough data at different ionic strengths and pH. The model developed was used to predict overloads and elution curves with high accuracy for a wide variety of gradients and different flow rates, and protein loads. The in-silico methodology used in this work for parameter estimation, along with a minimal amount of experimental data, can help the industry adopt model-based optimization and control of preparative ion-exchange chromatography with high accuracy.
Suggested Reviewers:	Giorgio Carta gc@eservices.virginia.edu
	Douglas Frey dfrey1@umbc.edu
	Massimo Morbidelli massimo.morbidelli@chem.ethz.ch
Opposed Reviewers:	

Powered by Editorial Manager® and ProduXion Manager® from Aries Systems Corporation

UNIVERSITY OF DELAWARE
Department of Chemical
& Biomolecular Engineering

University of Delaware
Newark, DE 19716-3110
Phone: 302-831-2543
Fax: 302-831-1048

August 23, 2021

Editorial Office
Journal of Chromatography A
P. O. Box 681
1000 AR Amsterdam
NETHERLANDS

Dear Sirs,

We are submitting the attached manuscript, titled "Robust mechanistic modeling of protein ion-exchange chromatography using a colloidal isotherm", to be considered for publication in the *Journal of Chromatography A.* The manuscript is of course in a topical area that has been widely covered in the journal but we believe that the performance that it describes represents a significant advance to the field. In addition, it describes a novel approach to determining model parameters independently of fitting the elution curves but demonstrating excellent accuracy in predicting such curves nonetheless. We also believe that the manuscript may be suitable for consideration for the virtual special issue on Downstream Processing for Purification of Protein Products, for which I received an invitation from Dr. Poole.

None of the present results have been submitted elsewhere for publication. I can be contacted by phone at +1-302-831-8989 and by e-mail at lenhoff@udel.edu. Thank you for your consideration.

Yours sincerely,

Abraham M. Lenhoff
Allan P. Colburn Professor

Highlights

- Mechanistic modeling framework presented for protein ion-exchange chromatography
- General rate model used with both pore and surface diffusion
- Breakthrough curves used for parameter estimation independently of elution
- Excellent elution prediction seen, including dependence on pH and ionic strength

Robust mechanistic modeling of protein ion-exchange chromatography using a colloidal isotherm

Vijesh Kumar[1], Samuel Leweke[2], William Heymann[2], Eric von Lieres[2], Fabrice Schlegel[3], Karin Westerberg[4], Abraham M. Lenhoff[1,*]

[1] Department of Chemical and Biomolecular Engineering, University of Delaware, Newark, DE 19716, USA

[2] Forschungszentrum Jülich GmbH, 52425 Jülich, Germany

[3] Amgen Process Development, One Kendall Square, 360 Binney St., Cambridge, MA 02141, United States

[4] Amgen Process Development, One Amgen Center Drive, Thousand Oaks, CA 91360, United States

* Corresponding author. E-mail lenhoff@udel.edu; phone +1 302 831 8989.

Abstract

Mechanistic models for ion-exchange chromatography of proteins are well-established and a broad consensus exists on most aspects of the detailed mathematical and physical description. A variety of specializations of these models can typically capture the general locations of elution peaks, but discrepancies are often observed in peak position and shape, especially if the column load level is in the non-linear range. These discrepancies may prevent the use of models for high-fidelity predictive applications such as process characterization and development of high-purity and -productivity process steps. Our objective is to develop a sufficiently robust mechanistic framework to make both conventional and anomalous phenomena more readily predictable using model parameters that can be evaluated based on independent measurements or well-accepted correlations. This work demonstrates the implementation of this approach for industry-relevant case studies using both a model protein, lysozyme, and biopharmaceutical product monoclonal antibodies, using cation-exchange resins with a variety of architectures (SP Sepharose FF, Fractogel EMD SO_3^-, Capto S and Toyopearl SP650M). The modeling employs the general rate model with the extension of the surface diffusivity to be variable, as a function of ionic strength or binding affinity. A colloidal isotherm that accounts for protein-surface and protein-protein interactions independently was used, with each characterized by a parameter determined as a function of ionic strength and pH. Both of these isotherm parameters, along with the variable surface diffusivity, were successfully estimated using breakthrough data at different ionic strengths and pH. The model developed was used to predict overloads and elution curves with high accuracy for a wide variety of gradients and different flow rates, and protein loads. The in-silico methodology used in this work for parameter estimation, along with a minimal amount of experimental data, can help the industry adopt model-based optimization and control of preparative ion-exchange chromatography with high accuracy.

1. Introduction

The essential elements of modeling chromatographic behavior have been known for many decades but the use of modeling in process development has grown appreciably only recently, aided by the availability of efficient and user-friendly chromatographic computational software [1]. Developing ion-exchange chromatography (IEC) models for proteins, in particular monoclonal antibodies (mAbs), is a long-standing challenge due to the complex nature of interactions on the charged surface [2-4]. Although IEC models have improved significantly and retention times can be well predicted, an accurate description of peak shapes for high loads during salt gradient elution is elusive [5]. Correct prediction of such protein elution behavior in IEC depends on an accurate description of both transport and the adsorption isotherm. Transport models such as the general rate model are well established, incorporating details of mass transfer within the pore space as well as surface diffusion [6]. The resulting partial differential equations are solved numerically with high accuracy and short run times using modern code libraries [7].

Numerous descriptions of protein partitioning between the bulk and the solid surface of the resin are available in the literature. Although most are based on physical models, only a few are based on detailed descriptions of interactions at the molecular level that are plausibly appropriate for proteins. The models most widely-used for ion-exchange systems are the Langmuir and steric mass action (SMA) models [8-10], both of which assume noninteracting solutes arranged in a monolayer on a charged surface. The Langmuir model does not explicitly account for salt effects and therefore modified or empirical relations are incorporated when it is used to describe gradient elution for ion-exchange chromatography [11,12]. The SMA model is explicit in salt concentration and its variation with pH has also been accounted for [13]. Both the Langmuir and SMA models capture the normal shape of typical protein adsorption isotherms, but the physical assumptions underlying the two models may not be fully justified. One discrepancy is that adsorbed protein molecules are likely to interact with neighboring solutes when the resin is loaded close to saturation in preparative chromatography [14]; this may give rise to deviations from the observed isotherms [15]. An SMA model modified to allow for multistate binding has also been used but without any direct experimental evidence [16]. To account for lateral protein-protein interactions, various colloidal models have been used [17-20] that may provide a more detailed description of actual physical phenomena that apply, in particular, at high-load conditions [21]. Other models that have been used include an empirical isotherm fitted directly to adsorption measurements but without a physical interpretation for the representation [22].

Regardless of the model details, parameter estimation from column data is a challenge because of the intrinsic convolution of transport and adsorption. In principle, mechanistically-meaningful models pose a less difficult challenge for estimating the model parameters as some of the parameters can be calculated using theoretical considerations like the amino acid sequence and dissociation information [23] but such models are generally not yet sufficiently reliable to provide the requisite predictive detail. Charge screening due to the presence of ions can be calculated from colloidal principles in terms of the Debye parameter [24] but this requires information on the molecular structure of the adlayer that is rarely available.

It is therefore not always possible to calculate parameters a priori, and some or all of them are fitted to measured isotherms [18] or to the elution curve (inverse fit method) [11,12, 24, 25]. The most direct method to measure the isotherm is a conventional static method wherein the concentration of solute in the mobile phase is measured after batch equilibration and the concentration in the stationary phase is determined by mass balance [26]. Other techniques use the Yamamoto method, which uses on-column gradient elution data [27, 28]. The binding affinity, which determines the initial slope of the isotherm, is also estimated using moment calculations for an isocratic pulse or breakthrough load on-column [29,30]. However, these methods do not allow simultaneous estimation of the transport parameters because there are not enough degrees of freedom in the elution curve to estimate binding and transport parameters separately. Pore and surface diffusion are usually slow enough to be rate-limiting and hence impact the overall transport [31,32], while "film" mass transfer is generally fast in IEC, allowing some latitude in specifying the parameter value.

The phenomenon of pore diffusion in a resin bead is well established, but surface diffusion, also sometimes referred to as solid or homogeneous diffusion, has been less widely studied. Measurements of homogeneous diffusion [33-36] have usually been performed for protein uptake and not for protein elution, where the changing salt concentration during IEC gradient elution complicates the model.

Given the significance of transport parameters, especially for proteins that are larger in size, such as mAbs, along with the uncertainties inherent in currently-available isotherm models, defining best practices for column modeling should necessarily focus on detailed treatments. Simpler models such as lumped-rate models or inflexible traditional models of isotherms are unlikely to be adequate to predict the peak shape during elution, especially for saturated loading. In this work an isotherm based on a colloidal model, which includes protein-protein and protein-surface interactions, has been implemented along with the general rate model, which includes both pore and surface diffusion (the latter as a function of ionic strength or binding affinity). Estimation of parameters was performed from overloaded conditions of protein on the column, which enabled the simultaneous estimation of the surface diffusivity and key isotherm parameters.

2. Materials and methods

2.1 Chemicals and buffers

All chemicals were purchased from Fisher Scientific (Waltham, MA) and were used after dissolution in deionized water and filtration through 0.2 µm filters. Buffer stock solutions (0.5 M monobasic sodium phosphate, 0.5 M disodium hydrogen phosphate, 1 M sodium acetate, and 1 M acetic acid) were prepared at room temperature (23 ± 2 °C). Acidic and basic buffer stock solutions were mixed in volumes as calculated from the Henderson-Hasselbalch equation to attain the desired pH and dilutions were made to obtain the desired ionic strength. Elution buffers at a desired ionic strength were prepared by adding 3 M sodium chloride stock solution to the equilibration buffers.

2.2 Protein sample preparation

Lysozyme from chicken egg (molecular weight 14.3 kDa) was dissolved in sodium phosphate buffer at pH 6.5, with salt concentrations in the range 20 mM – 500 mM. The protein concentration was in the range 4.0 – 5.0 mg/mL for the different samples.

The mAb used was obtained from Amgen's manufacturing facility (Thousand Oaks, CA). The formulated mAb (160 mg/mL) was stored at –80 °C and was thawed and diluted immediately before use to 25 mg/mL and buffer-exchanged into sodium acetate buffer. A purified native variant of the mAb was obtained using a displacement method on Poros HS resin packed in a 36 mL column (three XK 16/20 columns from GE Healthcare, Uppsala, Sweden, of bed height 6 cm each, used in series), as described previously [37].

2.3 Chromatography runs

The resins SP Sepharose FF, Capto S (GE Healthcare, Uppsala, Sweden), Fractogel SO_3^- (MilliporeSigma, Germany) and Toyopearl SP 650M (Tosoh Biosciences, King of Prussia, PA) were slurry-packed in columns of dimension 0.35 x 5 cm (Omnifit, Diba Industries Inc., CT, USA). An Äkta Pure chromatography system with a UV detector, conductivity meter, pH meter, and fraction collector was used for all the experiments. Protein samples were injected using a GE 50 mL Superloop if the sample volume was more than 500 µL. Chromatography was performed in two modes, breakthrough isocratic and linear gradient elution, at flow rates of 85-300 cm/h. The chromatography runs required two buffers, A and B. Buffer A was phosphate (for pH > 6.2) or acetate buffer (for pH < 6.2) and buffer B was buffer A adjusted to the desired ionic strength using 3 M sodium chloride. Buffer A in combination with varying percentages (0 - 100) of B was used for equilibration and washing during the chromatography runs.

The mAb was buffer-exchanged using Sephadex G-25 resin (GE Healthcare, Uppsala, Sweden) into the equilibration buffer prior to sample loading. The column was equilibrated with at least 5 column volumes (CVs) of buffer to obtain the desired pH and conductivity. The load volume for pulse experiments was 25 µL. For breakthrough experiments, which were used for estimating model parameters, the sample was loaded until the output concentration was close to the input concentration. After loading, the column was washed with the equilibration buffer until a stable baseline UV reading was obtained (A_{280}). Elution was performed in a salt gradient by combination of the equilibrium buffer with the B buffer. The column was regenerated and sanitized with 1 M NaCl and 0.5 M NaOH, respectively, after every five runs.

Gradient experiments followed a procedure similar to that described above except that the protein load was kept below the saturated capacity of the packed column. Elution was performed using salt gradients with different slopes (20, 30 or 40 CVs) prepared with B buffer as required for the various experiments. The data from these experiments were used for model validation aimed at various loading and elution conditions.

2.4 System and column calibration

2.4.1 UV detector

Samples of concentration 0.05 mg/mL to 25 mg/mL were prepared in buffer A and injected into the UV absorbance detector on the Äkta system. Measurements were made at 295 nm instead of 280 nm to obtain a broader linear range. The UV response measured in mAU was plotted against the concentration of protein injected. A second-order polynomial was fitted to the calibration curve to include the higher range near saturation of the UV detector. The concentration in mM of the sample eluted from the column was determined from the detector UV trace and the calibration curve.

2.4.2 Conductivity meter

Buffer A with varying percentages of buffer B was injected into the conductivity meter and a calibration curve was prepared for ionic strength (mM) versus conductivity (mS/cm). The conductivity trace was used to verify the ionic concentration at the column outlet during chromatography runs.

2.4.3 System hold-up volume

The holdup volumes in the tubing between the injection loop and the UV detector and between the gradient mixer and the UV detector were calculated by injecting dextran

(3000 kDa) without a column connected to the Äkta system. The retention time of the peak maximum was used to estimate the retention volume of the tubing.

2.4.4 Column interstitial porosity

The column interstitial porosity was determined based on the retention of dextran (3000 kDa). The retention time of the peak maximum was used to estimate the retention volume, and hence the interstitial porosity was calculated. The resin bead pore porosity was taken from the literature [38].

2.4.5 Column dispersion coefficient

The column dispersion coefficient was estimated from the peak shape of the protein under non-binding conditions (500 mM salt) on the column. A dispersion coefficient of 3.9 x 10^{-7} m^2/s was obtained by fitting a column model to a pulse peak shape using column simulations in CADET (section 2.7). The film mass-transfer coefficient was not transport-limiting and hence was set at 10^{-5} m/s for all the simulations [39].

2.5 General rate model

The general rate model was used as an adsorption and mass-transfer model for IEC. For a column of length *L* filled with spherical particles of radius r_p, the mass balances for the interstitial volume and porous beads respectively can be expressed as [6]

$$\frac{\partial c_i}{\partial t} = -u\frac{\partial c_i}{\partial z} + D_{ax}\frac{\partial^2 c_i}{\partial z^2} - \frac{1-\epsilon_c}{\epsilon_c}\frac{3}{r_p}k_{film,i}\left[c_i - c_{pi}\left(\cdot,\cdot,r_p\right)\right] \quad \text{for } t \geq 0,\ z \in [0,L] \qquad (1)$$

$$\frac{\partial c_{pi}}{\partial t} = D_{pi}\left(\frac{\partial^2 c_{pi}}{\partial r^2} + \frac{2}{r}\frac{\partial c_{pi}}{\partial r}\right) + D_{si}\frac{1-\epsilon_p}{\epsilon_p}\left(\frac{\partial^2 q_i}{\partial r^2} + \frac{2}{r}\frac{\partial q_i}{\partial r}\right) - \frac{1-\epsilon_p}{\epsilon_p}\frac{\partial q_i}{\partial t} \quad \text{for } t \geq 0,\ z \in [0,L] \text{ and } r \in [0,r_p] \qquad (2)$$

where c_i denotes the concentration of solute *i* in the interstitial space and c_{pi} and q_i the mobile- and solid-phase concentrations respectively of component *i* in the beads. The external porosity is given by ϵ_c and the internal porosity by ϵ_p, u denotes the interstitial velocity, D_{ax} the dispersion coefficient, $k_{film,i}$ the film mass-transfer coefficient, D_{pi} the pore diffusion coefficient and D_{si} the surface diffusion coefficient. D_{si} was treated as a function of the ionic strength in the bulk

$$D_{si} = D_{s0i} f(IS) \tag{3}$$

where D_{s0i} is a constant. The general rate model was coupled with the colloidal isotherm (section 2.6) to obtain the solution for the concentration profile at the end of the column, with the rate of adsorption given by

$$\frac{dq_i}{dt} = k_{kin}\,(c_{pi} - c_{pi}^*) \tag{4}$$

where k_{kin} is the adsorption rate constant and $c_{pi}{}^*$ is the concentration of protein in the pore space in equilibrium with q_i. The k_{kin} value was set to a high value (> 10^8 s^{-1}) for a rapid equilibrium model.

2.6 Colloidal isotherm model

For the colloidal isotherm model, the adsorbed protein molecules (concentration q_{i}) are assumed to be evenly distributed in a hexagonal arrangement on the surface at equilibrium, with the coverage varied via adjustment of the lattice size [17]. Protein-surface interactions are characterized by the equilibrium constant K_{e}, which gives rise to a linear equilibrium relation between c_{pi}^* and the protein concentration q_{i} in the bulk phase in the absence of lateral protein-protein interactions. At higher coverages such protein-protein interactions modulate the surface coverage via a protein-protein interaction parameter B_{pp}, a screening parameter κ, the protein radius a and the protein-protein spacing R. The colloidal model for a single component can then be written as [17]

$$q_i = K_e c_{pi}^* exp\left(-\frac{3}{2}\frac{B_{pp}a}{R} exp[-\kappa(R-2a)](3+\kappa R)\right) \tag{5}$$

Since the protein-protein interactions characterized by B_{pp} are long-ranged, they are assumed to be primarily electrostatic, with the range of interactions determined by the screening parameter, κ. The dependence of the model on solution conditions was modulated by adjusting the parameters κ, K_{e}, and B_{pp} as a function of ionic strength and pH.

2.7 Model simulations

Simulations were performed using a customized version of CADET (Chromatography Analysis and Design Toolkit), which included the colloidal isotherm and variable surface diffusivity, made available by Forschungszentrum Jülich, Germany [40]. The discretization was set to 150 axial nodes for a column of length 5 cm. The bead-level discretization was set to 100 radial nodes. The absolute tolerance was set to 10^{-8} and the relative tolerance to 10^{-6}.

2.7.1 Parameter estimation from inverse fit methods

Isotherm parameters were estimated by fitting simulation results to protein breakthrough data acquired in column experiments under isocratic conditions. The data points considered in calculating the residuals between the simulated and experimental data (normalized by input concentration) were for the protein loading and column wash stages rather than for elution experiments. Initial estimates of parameter values were obtained manually based on heuristic observations of the breakthrough shape. The initial guesses were then refined by minimizing the residuals using the MATLAB *lsqnonlin* function using the inverse fit method [11].

A variant of this approach used a weighting method in which the calculation of residuals was modified by including weighting values for ranges of data points on the breakthrough curve based on their sensitivities to specific model parameters. This method is based on the analysis of breakthrough curves discussed in detail in the Results and Discussion section. The confidence intervals for parameters were estimated using diagonal values of the covariance matrix obtained from the Jacobian and the variance of residuals from the output of the *lsqnonlin* function in Matlab. The significance levels were kept at 0.05 and the number of degrees of freedom was the number of iterations in the *lsqnonlin* optimization.

2.8 Estimation of isotherm parameters

The isotherm equation (5) incorporates several parameters that must be determined independently. The protein spacing, R, is premised on assuming a hexagonal monolayer arrangement [26], from which

$$R = \left(\frac{2}{\frac{\sqrt{3}\,(q_i N_A)}{\varphi}} \right)^{\frac{1}{2}} \qquad (6)$$

where q_i is the adsorbed protein concentration in volumetric units (mM), φ is the phase ratio and N_A is Avogadro's number.

The phase ratio can be expressed in various different forms and units. For adsorption on a conventional adsorbent, i.e., on an extended surface, the phase ratio $\boldsymbol{\varphi}$ is conveniently defined as an accessible surface area per unit volume of the mobile phase [38]. The phase ratio used here, denoted φ, is different to keep it consistent with the general rate model implemented in CADET. It is therefore defined as the accessible surface area per unit volume of solid. The phase ratio can be estimated from inverse size-exclusion chromatography (iSEC) and can be converted to φ using the value of the total porosity, ε_t:

$$\varphi = \boldsymbol{\varphi}(1 - \varepsilon_t)/(\varepsilon_t) \qquad (7)$$

The phase ratio measured using iSEC for Fractogel, a tentacular resin, will not be representative due to the nature of the sorbent, which lacks a well-defined surface area. For this case the phase ratio was estimated from Eq. 6 using the assumption that at the maximum binding capacity $q_{i,max}$, the protein-protein distance R has a minimum at $2a$ for monolayer adsorption, where a is the radius of the protein, the approximate value of which can be taken from the literature [41]:

$$\varphi = 2\sqrt{3}\, a^2\, q_{i,\,max}\, N_A \qquad (8)$$

For this situation $q_{i,max}$ was calculated from the amount of bound protein determined from the column breakthrough data.

The screening or Debye parameter (κ) for protein-protein interactions was estimated assuming the colloidal behavior of protein in an electrolyte solution of a symmetric monovalent salt (NaCl). The total ionic strength C_0 was accounted for due to the presence of salt only, independent of the presence of protein, in the bulk phase. The functional relationship of κ with ionic strength takes the form

$$\kappa = \kappa_0 \, (C_0)^{0.5} \tag{9}$$

where κ_0 at 298 K is 1.04x10^8 m^{-1}.

The other two isotherm parameters, K_e and B_{pp}, were not obtained from theoretical considerations but were determined empirically by fitting each isocratic breakthrough curve individually at constant salt and protein concentration. The global ionic strength dependence of K_e and B_{pp} was then obtained by fitting a three-parameter power law (k_4, b_4 = 0) or exponential function (k_2, b_2 = 0) to the individual estimated values of total ionic strength :

$$\ln K_e = k_1 C_0^{-k2} + k_3 \exp(k_4 C_0) \tag{10}$$

$$B_{pp} = b_1 C_0^{b2} + b_3 \exp(b_4 C_0) \tag{11}$$

where k_1, k_2, k_3, k_4, b_1 b_2, b_3, and b_4 are fitting constants.

2.9 Estimation of transport parameters

The external mass transfer coefficient $k_{film,i}$ is known to have the smallest effect on column behavior in ion-exchange chromatography of proteins [39], so it was assumed in this work to have a relatively high value, 10^{-5} m/s.

The pore diffusivity D_p inside the particle was calculated approximately from [42]

$$D_p = \frac{\varepsilon_p \omega}{\tau} D_0 \tag{12}$$

where D_0 is the free-solution diffusivity, ε_p is the accessible pore porosity, ω is the hindrance coefficient and τ is the tortuosity. The hindrance coefficient was set to 1 because the resins used here had mean pore sizes significantly larger than the protein dimensions, and the tortuosity was set to 3, recognizing the typical range of tortuosity of 2-6 [43]. This initial approximation of D_p was further fine-tuned by fitting to the breakthrough data.

The surface diffusivity was estimated using the breakthrough data as outlined in Results and Discussion.

3. Results and discussion

3.1 Peak shapes for different systems

The shape of the elution peak depends strongly on the protein load on the column and may deviate appreciably from the near-Gaussian shape expected at low loads. Whether a load is considered low or high can vary with the resin and the protein and depends on the resin dynamic capacity, which in turn depends in part on the protein binding affinity and on resin structural and transport properties. The experimentally-observed gradient elution behavior of lysozyme, cytochrome c, and a mAb with increasing load is shown in Fig. 1. In general, as the load increases, elution is expected to start earlier, so the peak spread should be leftward, with a close approximation to a Gaussian peak shape. This is observed for the small protein lysozyme on SP Sepharose FF (Fig. 1A) but anomalies are observed for other cases. In the case of the mAb, although the peaks are symmetric and near-Gaussian, the peak spread is both leftward and rightward with increasing load (Fig. 1B and C). Lysozyme on Capto SP ImpRes produces a leftward spread but with a kink at saturated loading (Fig. 1D). In more atypical observations asymmetric peaks (forward and backward tilt) are observed for cytochrome c and lysozyme on Fractogel SO_3^- (Fig. 1E and F).

The shape of the peak is likely related to the isotherm shape and to how it changes with ionic strength [1]. Although the peak spread also depends on the isotherm behavior, it may be related more to the transport in the pore space, especially for the large mAb. This could be due to limitations in either pore or surface diffusion or both. When the mAb was loaded at a higher ionic strength (Fig. 1C), only a leftward spread was seen, suggesting that the effect is related to the binding affinity and hence possibly to surface diffusion. These results, taken together, emphasize the importance for accurate prediction of chromatographic behavior of accurately determining both the isotherm and transport parameters.

3.2 Analysis of breakthrough curves

Although the shapes of the elution peaks in Fig. 1 may reflect effects of surface diffusion, such effects can be inferred more reliably from breakthrough (BT) data for a range of ionic strengths (IS, 40-150 mM) (Fig. 2A). The curvature and steepness of the breakthrough curve reflect protein uptake in the column, which takes longer to reach saturation capacity at lower ionic strength, indicating slower transport. At very low IS (40 mM) the breakthrough starts earlier than at 60 mM but also with slower protein uptake. At higher ionic strength, uptake is faster, so saturation capacity is reached in a shorter time, albeit with a lower saturation load because of the lower equilibrium capacity.

3.2.1 Breakthrough data for estimation of surface diffusivity

Simulated breakthrough curves at fixed ionic strength but varying surface diffusivity are shown in Fig. 2B, which further supports the assertion that this behavior can be modeled by including surface diffusion as a function of IS in the general rate model. Previous studies [34,44,45] also support the argument that the surface diffusivity indeed varies with ionic strength. However, estimation of the surface diffusivity from column data independent of other transport parameters remains a challenge.

The surface diffusivity was estimated based on the curvature of the front of the BT curve. The uptake slope is shallower at low than at higher IS, presumably due to transport limitations. Changes in pore diffusivity can be ruled out as there is no change in porosity in the given salt range, although electrostatic exclusion [46] may contribute to a reduced pore diffusivity. The latter is unlikely to be the principal explanation, however, as the effect is seen even in adsorbents of which the pore size is too large for exclusion to be significant. This leaves surface diffusion as the likely explanation, and indeed the dependence of surface diffusivity on ionic strength has also previously been observed and modeled [44,45]. The surface diffusion contribution to transport is enhanced at high surface coverage and hence the surface diffusivity can be estimated from the curvature of the front of the breakthrough curve. The variations in the shape of the curve with changing values of surface diffusivity can be simulated by the model (Fig. 2B).

3.2.2 Breakthrough data for estimation of isotherm parameters

Estimation of the surface diffusivity is further complicated by the need also to estimate isotherm parameters, which for preparative chromatography models must be accurate even in the nonlinear (plateau) region. Even for feed concentrations as low as 1 mg/mL, typical isotherms at low IS will result in resin at the top of the column experiencing local saturation, so it would be informative to know the protein binding profile along the length of the column (Fig. 2C). In the (usual) absence of such data, a breakthrough curve represents an extrapolation of this behavior to the end of the column, with protein loaded until the effluent concentration reaches a plateau, followed by a chase with wash buffer. In this section we show via simulations how the shape of the breakthrough curve is related to changes in various model parameters, using the colloidal isotherm.

The transport (D_s) and isotherm (K_e and B_pp) parameters were fitted to the breakthrough data simultaneously using the inverse fit method [11]. This procedure was more effective if different weights were assigned to different parts of the breakthrough curve for its dependence on model parameters (section 2.7.1). Adsorption behavior is most sensitive to K_e (initial slope of isotherm) when either c_{pi} or q_i is close to zero. At low ionic strengths, adsorption is strong and transport-limited, so it is difficult to reach conditions for which q_i is low except in the complete absence of protein locally. In contrast, a low c_{pi} condition is readily encountered after protein loading is stopped and the column is washed with buffer, during which re-equilibration gives rise to continuous desorption and hence a finite effluent c_{pi} that decreases with time, ultimately approaching zero. Consequently, the slope of this tail of the breakthrough curve is a measure of sensitivity to K_e. The drop in c_{pi} is faster at lower than at higher ionic strength. This part of the BT curve is also not very sensitive to the surface diffusivity value, which hence does not interfere with the estimation of K_e.

The retention time of the front of the breakthrough curve is a more sensitive measure of protein binding capacity and hence more sensitive to the protein-protein interaction parameter B_{pp}. The sensitivity of the breakthrough shape to K_e and B_{pp} is shown in Fig. 2, with the maximum capacity kept fixed in Fig. 2D and K_e kept fixed in Fig. 2E.

Therefore, to estimate the three parameters (K_e, B_{pp}, and D_s), we use breakthrough data, but in three distinct regions: (1) The retention of the front is sensitive to B_{pp}, (2) the curvature of the tail is sensitive to K_e, and (3) the curvature of the front is sensitive to D_s given that the pore diffusivity is assumed to be constant.

3.3 Lysozyme on Capto SP ImpRes

Using the colloidal isotherm (Eq. 5) to model lysozyme behavior on Capto SP ImpRes provides an informative application of the approach outlined above. The fitting parameters K_e, B_{pp}, and D_s were estimated from isocratic breakthrough data at five different IS values following the procedure described in section 3.2. Other parameters, specifically the Debye screening parameter and the pore diffusivity, were calculated from theoretical correlations (Eqs. 9 and 12 respectively). The phase ratio for Capto ImpRes was estimated from Eq. 8, as no literature data were available. The maximum binding capacity required in Eq. 8 was calculated from the area above the breakthrough curve at 30 mM IS until it reached its plateau. With these calculated parameters and optimal fits of K_e, B_{pp}, and D_s for each IS, the simulated breakthrough curves, along with experimental data, are shown in Fig. 3A.

The isotherm parameters are plotted against ionic strength (at pH 7.0) in Fig. 3B, with both showing a monotonic decrease consistent with weakening protein-surface and protein-protein interactions with increasing IS. Both B_{pp} and K_e fit a power-law form as a function of IS (Eqs. 10 and 11). The 3D isotherm surface, calculated from the estimated parameters and showing dependence on both the mobile-phase protein concentration and IS, is shown in Fig. 3C. The fitted surface diffusivity, D_s, was found to be negligible in the 30-200 mM range of IS but increased significantly in the 200-400 mM range and was found to depend exponentially on IS (Fig. 3E).

The gradient elution behavior predicted using this set of parameters is shown in Fig. 3D along with the corresponding experimental data; all the predictions agree well with the data even though none of the elution data were used for parameter estimation. The model was also verified for different gradient slopes (data not shown). It is interesting to observe that with increasing load, a kink started to appear on the front of the gradient elution peak and is also very well captured by the model. This behavior may result from the shape of the isotherm curve with changing IS (Fig. 3C); this is discussed in comparison to the near-Gaussian elution peaks seen for mAbs in section 3.6.

3.4 MAb on Fractogel: Deviations from colloidal isotherm model

Initial efforts to model breakthrough data for the mAb on Fractogel did not provide a satisfactory quality of fit. Specifically, for higher IS (130-175 mM) the breakthrough front could be captured accurately but values of K_e and B_{pp} that could match the slope of the tail of the breakthough curve could not be obtained reliably. To ensure that the discrepancy observed was not due to errors in values of kinetic or transport parameters, the model was extensively tested with these parameters varied in a reasonable range, but none of these produced the desired fit. The best fits obtained along with experimental data for the mAb at pH 5.0 are shown in Fig. 4A. The deviations, although not very large, are more pronounced at pH 5.0 than at pH 5.5 or 6.0, probably because of the higher IS range of interest for the mAb at lower pH. Although the deviations could be ameliorated by optimizing the fits in the tails of the BT curves, the resulting B_{pp} values showed an upturn at higher IS (cf. Fig. 3 for lysozyme) that complicated column simulations.

The colloidal isotherm formulation [17,18] is based on an idealized physical model in which protein adsorption is modeled as occurring in a monolayer of hexagonally-ordered spheres. The colloidal isotherm, like any other, incorporates various idealizations, and its application especially in the present system, involving the highly-anisotropic mAb shape, represents use of the mathematical isotherm form more than the physical idealization. In that sense the model may not adequately capture the details of the experimental isotherm shape, to which column model predictions are highly sensitive. Parametric exploration showed that improved fits could be obtained by treating the screening parameter, κ, as a constant for a given system instead of using the explicit IS dependence given in Eq. 9. Although larger deviations were seen only at higher IS, where the Debye screening length κ^{-1}, calculated from Eq. 9, is < 1 nm, the constant-κ formulation was used for all mAb modeling.

The screening parameter, κ, was therefore treated as adjustable for a given system and was fitted to breakthrough data along with the other isotherm parameters (K_e and B_{pp}). The model was able to the fit data very well for screening parameter values $\kappa < 0.4$ nm^{-1} ($\kappa^{-1} > 2.5$ nm) for higher ranges of IS (> 150 mM) and < 1.33 nm^{-1} ($\kappa^{-1} > 0.75$ nm) for lower salt ranges (< 100 mM). Both the use of constant values of κ generally as well as the decrease in the screening parameter with increasing IS are inconsistent with the tenets of colloid theory. Although it is possible that there is a physical explanation for these observations, it is reasonable instead to regard the isotherm model simply as a mathematical formalism, as noted above.

Since reasonable fits were obtained for not only one value of κ^{-1} but for a range (1.5 to 4.5 nm) of values, estimating a single set of parameters for an isotherm becomes somewhat arbitrary. The simplest solution was to keep the screening parameter fixed at one value for different ionic strengths, with a value slightly lower than that calculated from the Debye relation (Eq. 9) found to be most effective. This method may not be universal but provides reasonable trends for the other parameters and hence a working model that we have found effective for mAbs on different stationary phases. To obtain a sense of the best value of κ^{-1}, breakthrough curves were fitted for values of κ^{-1} spaced at intervals of 0.5 nm, with adjustment of the other two isotherm parameters, K_e and B_{pp}. The residual plot (RMSD) is shown in Fig. 4B and the trends in fitted values of K_e and B_{pp} in Fig. 4C and D respectively. The latter two plots both show similar monotonically-decreasing trends (cf. Fig. 3B), albeit with appreciable differences in values. A final value of κ^{-1} of 2.5 nm was found to be best based on the minimum in the residual for the entire range of IS and pH.

3.5 MAb on Fractogel: transport properties and porosity

Beyond the isotherm parameters, the shape of the breakthrough curve is also affected by transport properties. Furthermore, the pore diffusivity estimate depends directly on the particle porosity, ε_p (Eq. 12), and because the porosity affects the phase ratio and hence the amount of adsorbed protein, the estimated value of the surface diffusivity also changes with ε_p. Initial estimates of ε_p were taken from literature values that were estimated from inverse size exclusion chromatography (iSEC) data [38], so some uncertainty remains in the values obtained. For Fractogel specifically, the presence of tentacles adds uncertainty to how the porosity affects the physical behavior.

The breakthrough curves were fitted using the isotherm parameters and the surface diffusivity as adjustable parameters, but the porosity was also fine-tuned from the initial estimate. This helped predominantly in reducing the residual error in fitting simulated breakthrough curves at low IS, particularly in the plateau region, where the column reaches the saturation limit. The porosity was the only realistic parameter that could be changed (up to ± 25%) to improve the fit in this portion of the breakthrough curve.

To further validate the estimated values of the surface diffusivity and the porosity, the predictive capability was tested for breakthrough curves at two additional flow rates (84 and 300 cm/hr). The parameters obtained from the fit at the base flow rate of 150 cm/hr were able to provide reasonable predictions of the breakthrough curves at the other two flow rates while keeping all other model parameters identical (Fig. 5), validating the utility of the correction to the porosity value.

As discussed previously, the surface diffusivity depends on IS. The functional form of this dependence obtained for all pH values was exponentially increasing and described by the two-parameter form

$$D_s = D_{sf} \exp(C_0 D_{sc}) \qquad (13)$$

where D_{sf} and D_{sc} are fitted parameters. This functional form can be used to estimate the value of the surface diffusivity in cases for which breakthrough data are partial or incomplete. The functional relation can also be useful for fitting breakthrough data at higher IS, where the effect of the surface diffusivity on the curvature of the uptake profile is confounded with the effect of K_e. In this limit there is also less impact of B_{pp} than at lower ionic strength or at higher protein coverage.

3.6 Parameter estimates and model predictions for mAb on Fractogel

Combining the approaches described in sections 3.5 and 3.6 leads to the breakthrough calibration data at pH 5.5 shown in Fig. 6A, where a constant screening length value of 2.5 nm was used. The parameter values obtained by fitting an individual breakthrough curve (i.e., at one set of conditions) were also adjusted based on validation assessment from the elution peak obtained after the same breakthrough curve. The estimates at individual conditions were then fitted to more global forms as a function of IS (Eqs. 10 and 11), with iterative adjustments made to obtain a smooth trend with power-law or exponential dependence. Once the final values were obtained, confidence intervals (CI) were calculated (section 2.7.1) and it was observed that in most cases the values obtained using the global correlations remained within the CI range for individual points.

For the breakthrough curves at pH 5.5 (Fig. 6A), the dynamic binding capacity at low salt (44 mM) is lower than at higher IS (95 mM). The reason is apparent in the 3D isotherm shape (Fig. 6G), namely the local maximum on the surface with changing IS, i.e., a local maximum in the equilibrium binding capacity. The fitted values of K_e and B_{pp} (Fig. 6B, C) and of D_s (Fig. 6E) as a function of IS show that both the B_{pp} and D_s trends superimpose if plotted against K_e (Fig. 6D, F). The B_{pp} dependence is reasonable given that both protein-surface interactions and protein-protein interactions are predominantly electrostatic and depend on the protein charge and on solution conditions. The relation between D_s and K_e has been discussed previously [34, 44].

The elution predictions were validated for a wide range of conditions, for which a few selected profiles are shown in Fig. 7. The final model was also able to capture partial (e.g., Fig. 7C) and complete breakthrough in the elution profiles with a single set of unique parameters. The effects of the gradient slope, flow rate, and load capacity are accurately captured by the model. Predictions for other conditions (pH 5.0 and 6.0) are provided in the supplementary information and show similar performance in predicting elution behavior, including for step elution. No kinks were observed in the elution peak profiles with higher loads for mAbs, as was present for lysozyme on Capto SP ImpRes (Fig. 3D). The likely reason is the difference in isotherm shapes, as the 3D isotherm surface for lysozyme on this resin (Fig. 3E) was monotonically decreasing with IS, which is different to the case for the mAb on Fractogel (Fig. 6G - I).

3.7 pH dependence

The pH is an important process variable in determining the robustness and load performance of mAbs on IEX resins. The model described above does not explicitly include the effect of pH and hence cannot be used to predict minor perturbations during the process. To overcome this limitation, the pH effect was incorporated in the model by parameterizing K_e and B_{pp} as a function of pH in addition to the ionic strength dependence. The functional form of the pH dependence was determined by fitting the breakthrough data separately at pH 5.0, 5.5 and 6.0 for different ionic strengths and combining them in the form

$$\ln(K_e) = \alpha\left[C_0^{\beta} + \gamma\right]\left[pH^{\delta}\right] \tag{14}$$

where $\alpha,\ \beta,\ \gamma$ and δ are fitting parameters. Eq. 14 fits the ln K_e data (Fig. 8A) well except for a slight deviation in the fit at higher salt and pH, but this does not significantly affect elution predictions because these are essentially non-binding conditions.

B_{pp} is linearly related to ln K_e at higher binding affinities but not at lower affinities; the latter deviations are evident at higher pH and ionic strength in results shown earlier (Fig. 6D). However, for weaker binding the contribution of protein-protein interactions would not play a significant role due to lower coverages, so B_{pp} can be assumed to depend linearly on ln K_e more generally. For more accurate predictions, a power-law formalism similar to that for K_e (Eq. 14) in terms of C_0 is effective:

$$B_{pp} = \alpha'\left[C_0^{\beta'} + \gamma'\right]\left[pH^{\delta'}\right] \tag{15}$$

As discussed in the previous section D_s depends explicitly on K_e, so a separate equation is not required in terms of IS or pH but only in terms of K_e [44],

$$D_s = d_1 (\ln K_e)^{d_2} \tag{16}$$

where d_1 and d_2 are power-law parameters.

3.8 Isotherm model for mAb on other resins

Model calibration and validation were also performed on a variety of other resins. To examine differences on a family of related resins, the results on Fractogel were augmented by corresponding ones on custom Fractogel variants with low (395 μeq/g) and high ligand densities (645 μeq/g) relative to the standard version (541 μeq/g) [47]. Isotherm parameters (K_e and B_{pp}) fitted to breakthrough curves at pH 5.0 and 5.5 are compared in Fig. 9A-D for the two Fractogel variants and the standard version. The higher ligand-density resin showed a higher binding affinity and greater protein – protein repulsion as expected. The ln K_e and B_{pp} values for different ligand densities, at both pH 5.0 and 5.5, converge with increasing IS, but the ln K_e curves are more nearly parallel for the two pH values. This indicates that ligand density plays a more important role at lower ionic strength, irrespective of pH, but the effect is attenuated at higher ionic strength. The behavior of the protein-protein interaction parameter, B_{pp}, is different between pH 5.0 and pH 5.5, which is not observed for K_e (Fig. 9B, D). Although the trends in B_{pp} are roughly similar, the behavior at the higher pH, where the curves for the standard and high ligand-density resins almost overlap, is not seen at the lower pH. The surface diffusivity values, however, all superimpose as a function of K_e and show a strong correlation irrespective of pH and ligand density (Fig. 9G). Breathrough and elution predictions and fits are provided in the supplementary information.

To explore a wider range of resin architectures, parameters for the mAb on SP Sepharose FF, Capto S, and Toyopearl SP650 at pH 5.0 are presented in Fig. 9E-F. The trends observed for these resins are similar to those for Fractogel, but both the binding affinity and protein-protein interaction parameter are lower, which may be due to differences in ligand density, phase ratio or other resin properties. The plots of ln K_e vs. IS are almost parallel, indicating that they reflect characteristics of the protein [48]. The surface diffusivity values again all follow a power-law function of binding affinity irrespective of resin backbone/surface (Fig. 9H). This implies that the model formulation with respect to binding affinity, protein-protein interaction, and surface diffusivity reflects a universal trend and form. This also demonstrates that the method proposed here for parameter estimation can work equally well for a wide variety of resins and pH conditions.

3.9 Model applications and limitations

The methods developed in this work aim to provide a modeling framework for a wide range of operating conditions, including pH, flow rate, gradient, and overload effects. The overload element will also be useful for multicolumn setups, where the column capacity has to be established accurately. Overloading is also important in displacement and frontal chromatography, where multicomponent effects also enter the picture. In general, in most processes the column capacity is underutilized (~80%), so the benefits of displacement effects are often overlooked. Operating consistently at higher loads may reduce process robustness in the absence of accurate models to capture protein leakage due to changes in buffer composition and flow rate. Since the models developed here include all these important process parameters, more consistent usage of the full column capacity may be aided by adequate model capabilities.

The model here includes detailed transport effects, including pore and surface diffusion explicitly, in a fashion consistent with the findings of direct investigations of protein chromatographic transport; including these effects and their dependence on operational variables can help to predict transport limitations that are observed mainly at low ionic strengths. Models for ion-exchange chromatography are incomplete without including the effect of pH, as column behavior is much more sensitive to this than to ionic strength, at least for large molecules like mAbs. Accurate predictions of pH dependence will help to model process sensitivity to variations in solvent buffer composition in the process environment. The colloidal model used here segregates the protein-resin and protein-protein interaction parameters explicitly, which can be useful in troubleshooting as well as in extracting mechanistic insights, which are often obscured in other isotherm models.

This could thus help to elucidate protein behavior on the column based on the physicochemical and surface properties of the protein and the resin surface.

The biggest challenge in developing an effective model is not only in ascertaining the right formalism for the isotherm and transport but also in estimating the model parameters. Here we have shown an effective route to solve this problem with the use of the breakthrough curve, but this requires a fairly large amount of protein that, in many cases, would not be available for a process in the early development stage. However, as models for more proteins are generated, e.g., for different mAbs, a general trend can be established that leads to informative heuristics, and a full set of breakthrough curves may not be necessary. The model parameters may then be bounded in fairly narrow domains, and by using inverse fitting in gradient elution or machine learning methods, an accurate data model can be constructed.

In the approach described here we have estimated some parameters, e.g., the pore diffusivity, from theoretical correlations and then obtained others, e.g., the surface diffusivity, by fitting the breakthrough curves. The *a priori* estimates are susceptible to errors, such as the effect of particle porosity on pore diffusivity discussed earlier. In addition, the theoretical models used for such estimates may include idealizations from which the real physical system deviates in a way that would be difficult to account for accurately. For example, the colloidal model accounts for protein-protein interactions using a model of a monolayer of spheres in a hexagonal array, a very crude approximation of adsorbed mAb. Such idealizations may be compensated for in part by adjustable parameters but we have also used other adjustments empirically, such as using a constant value of the screening parameter. The value of 0.4 nm^{-1} was used throughout the work to calibrate the breakthrough data, but other values > 0.22 nm^{-1} also produced accurate fits, albeit with higher values of and sensitivity to the binding affinities estimated in the low ionic strength range. Although this includes some arbitrariness, we feel that it is a reasonable approach given the complexity of the mAb molecular structure and the resin surface. The end result is a working and extensively-verified model with reasonable and physically-meaningful parameter values, producing true and accurate predictions sufficiently robust to capture changes in flow rate, load, pH and other operating parameters. We were able to model the different peak shapes observed for the data presented in section 3.1, elucidating the importance of incorporating detailed transport and isotherm characteristics for protein chromatography modeling.

4. Conclusions

The general rate model is widely established for rigorous modeling of chromatographic behavior. We have shown that the specific implementation used here, with incorporation of the colloidal isotherm model and both pore and surface diffusion, captures the features of isocratic and gradient elution peak shape to a very high degree of accuracy. A key element is the fitting of breakthrough curves to obtain estimates of model parameters independently of the elution data, including revelation of relationships among model parameters by the shape of the protein front as it migrates through the column, as a function of binding affinity. The resulting model is capable of accurately predicting loading and elution for pulse to saturated loads using the same set of parameters. The transport predictions were sufficiently accurate to capture the peak shape and spread for different loads and flow rates. The methodology developed in this work, along with the implementation of the colloidal model inclusive of pH and ionic strength, will help the application of models for preparative chromatography in industrial applications.

Acknowledgments

We are grateful for the financial support of Amgen, Inc. and for the materials that the company provided that made the work possible. We are also grateful to MilliporeSigma for making possible the investigation of the performance of the Fractogel charge variants.

References

1. Kumar, V., & Lenhoff, A. M. (2020). Mechanistic Modeling of Preparative Column Chromatography for Biotherapeutics. *Annual Review of Chemical and Biomolecular Engineering*, *11*, 235-255.

2. Quan, X., Liu, J., & Zhou, J. (2019). Multiscale modeling and simulations of protein adsorption: progresses and perspectives. *Current Opinion in Colloid & Interface Science*, *41*, 74-85.

3. Hanke, A. T., & Ottens, M. (2014). Purifying biopharmaceuticals: knowledge-based chromatographic process development. *Trends in Biotechnology*, *32*(4), 210-220.

4. Guélat, B., Khalaf, R., Lattuada, M., Costioli, M., & Morbidelli, M. (2016). Protein adsorption on ion exchange resins and monoclonal antibody charge variant modulation. *Journal of Chromatography A*, *1447*, 82-91.

5. Creasy, A., Barker, G., Yao, Y., & Carta, G. (2015). Systematic interpolation method predicts protein chromatographic elution from batch isotherm data without a detailed mechanistic isotherm model. *Biotechnology Journal*, *10*(9), 1400-1411.

6. Schmidt-Traub, H. (2005). *Preparative Chromatography: Of Fine Chemicals and Pharmaceutical Agents.* Wiley-VCH Verlag GmbH & Co. KGaA, pp. 215-296.

7. von Lieres, E., & Andersson, J. (2010). A fast and accurate solver for the general rate model of column liquid chromatography. *Computers & Chemical Engineering*, *34*(8), 1180-1191.

8. Ruthven, D. M. (1984). *Principles of adsorption and adsorption processes*. John Wiley & Sons.

9. Lan, Q., Bassi, A. S., Zhu, J. X. J., & Margaritis, A. (2001). A modified Langmuir model for the prediction of the effects of ionic strength on the equilibrium characteristics of protein adsorption onto ion exchange/affinity adsorbents. *Chemical Engineering Journal*, 81(1-3), 179-186.

10. C.A. Brooks, S.M. Cramer Steric mass-action ion exchange: displacement profiles and induced salt gradients *AIChE J*., 38 (1992), pp. 1969-1978, 10.1002/aic.690381212

11. Kumar, V., Leweke, S., von Lieres, E., & Rathore, A. S. (2015). Mechanistic modeling of ion-exchange process chromatography of charge variants of monoclonal antibody products. *Journal of Chromatography A*, 1426, 140-153.

12. Kumar, V., & Rathore, A. S. (2017). Mechanistic modeling based PAT implementation for ion-exchange process chromatography of charge variants of monoclonal antibody products. *Biotechnology Journal*, *12*(9), 1700286.

13. Schmidt, M., Hafner, M., & Frech, C. (2014). Modeling of salt and pH gradient elution in ion-exchange chromatography. *Journal of Separation Science*, 37(1-2), 5-13.

14. Latour, R. A. (2015). The Langmuir isotherm: a commonly applied but misleading approach for the analysis of protein adsorption behavior. *Journal of Biomedical Materials Research Part A*, 103(3), 949-958.

15. Barker, G., Yao, Y., & Carta, G. (2015). Systematic interpolation method predicts protein chromatographic elution from batch isotherm data without a detailed mechanistic isotherm model. *Biotechnology Journal*, 10(9), 1400-1411.

16. Diedrich, J., Heymann, W., Leweke, S., Hunt, S., Todd, R., Kunert, C. von Lieres, E. (2017). Multi-state steric mass action model and case study on complex high loading behavior of mAb on ion exchange tentacle resin. *Journal of Chromatography A*, 1525, 60-70.

17. Oberholzer, M. R., & Lenhoff, A. M. (1999). Protein adsorption isotherms through colloidal energetics. *Langmuir*, 15(11), 3905-3914.

18. Xu, X., & Lenhoff, A. M. (2008). A predictive approach to correlating protein adsorption isotherms on ion-exchange media. *Journal of Physical Chemistry B*, 112(3), 1028-1040.

19. Guélat, B., Ströhlein, G., Lattuada, M., & Morbidelli, M. (2010). Electrostatic model for protein adsorption in ion-exchange chromatography and application to monoclonal antibodies, lysozyme and chymotrypsinogen A. *Journal of Chromatography A*, 1217(35), 5610-5621.

20. Guélat, B., Khalaf, R., Lattuada, M., Costioli, M., & Morbidelli, M. (2016). Protein adsorption on ion exchange resins and monoclonal antibody charge variant modulation. *Journal of Chromatography A*, *1447*, 82-91.

21. Guélat, B., Ströhlein, G., Lattuada, M., Delegrange, L., Valax, P., & Morbidelli, M. (2012). Simulation model for overloaded monoclonal antibody variants separations in ion-exchange chromatography. *Journal of Chromatography A*, 1253, 32-43.

22. Reck, J., Pabst, T., Hunter, A., Barker, G., & Carta, G. (2019). Systematic Interpolation Method Predicts Antibody Monomer-Dimer Separation by Gradient Elution Chromatography at High Protein Loads. *Biotechnology Journal*, 14(3), 1800132.

23. Roth, C. M., & Lenhoff, A. M. (1993). Electrostatic and van der Waals contributions to protein adsorption: computation of equilibrium constants. *Langmuir*, *9*(4), 962-972.

24. Osberghaus, A., Hepbildikler, S., Nath, S., Haindl, M., von Lieres, E., & Hubbuch, J. (2012). Determination of parameters for the steric mass action model—A comparison between two approaches. *Journal of Chromatography A*, *1233*, 54-65.

25. Borg, N., Westerberg, K., Andersson, N., von Lieres, E., & Nilsson, B. (2013). Effects of uncertainties in experimental conditions on the estimation of adsorption model parameters in preparative chromatography. *Computers & Chemical Engineering*, *55*, 148-157.

26. Xu, X., & Lenhoff, A. M. (2009). Binary adsorption of globular proteins on ion-exchange media. *Journal of Chromatography A*, *1216*(34), 6177-6195.

27. Yamamoto, S., Nakanishi, K., Matsuno, R., & Kamijubo, T. (1983). Ion exchange chromatography of proteins—predictions of elution curves and operating conditions. II. Experimental verification. *Biotechnology and Bioengineering*, *25*(5), 1373-1391.

28. Rüdt, M., Gillet, F., Heege, S., Hitzler, J., Kalbfuss, B., & Guélat, B. (2015). Combined Yamamoto approach for simultaneous estimation of adsorption isotherm and kinetic parameters in ion-exchange chromatography. *Journal of Chromatography A*, *1413*, 68-76.

29. Radeke, K. H., Ortlieb, H. J., & Gelbin, D. (1981). Evaluating breakthrough curves with the method of moments for systems obeying the Langmuir isotherm. *Chemical Engineering Science*, *36*(1), 11-17.

30. Liu, Z., Roininen, J., Pulkkinen, I., Sainio, T., & Alopaeus, V. (2013). Moment based weighted residual method—New numerical tool for a nonlinear multicomponent chromatographic general rate model. *Computers & Chemical Engineering*, *53*, 153-163.

31. Ma, Z., Whitley, R. D., & Wang, N. H. (1996). Pore and surface diffusion in multicomponent adsorption and liquid chromatography systems. *AIChE Journal*, *42*(5), 1244-1262.

32. Stone, M. C., Tao, Y., & Carta, G. (2009). Protein adsorption and transport in agarose and dextran-grafted agarose media for ion exchange chromatography: Effect of ionic strength and protein characteristics. *Journal of Chromatography A*, *1216*(20), 4465-4474.

33. Traylor, S. J., Xu, X., & Lenhoff, A. M. (2011). Shrinking-core modeling of binary chromatographic breakthrough. *Journal of Chromatography A*, *1218*(16), 2222-2231.

34. Lenhoff, A. M. (2008). Multiscale modeling of protein uptake patterns in chromatographic particles. *Langmuir*, *24*(12), 5991-5995.

35. Dziennik, S. R., Belcher, E. B., Barker, G. A., DeBergalis, M. J., Fernandez, S. E., & Lenhoff, A. M. (2003). Nondiffusive mechanisms enhance protein uptake rates in ion exchange particles. *Proceedings of the National Academy of Sciences*, *100*(2), 420-425.

36. Weaver Jr, L. E., & Carta, G. (1996). Protein adsorption on cation exchangers: comparison of macroporous and gel-composite media. *Biotechnology Progress*, 12(3), 342-355.

37. Khanal, O., Kumar, V., Westerberg, K., Schlegel, F., & Lenhoff, A. M. (2019). Multi-column displacement chromatography for separation of charge variants of monoclonal antibodies. *Journal of Chromatography A*, *1586*, 40-51.

38. DePhillips, P., & Lenhoff, A. M. (2000). Pore size distributions of cation-exchange adsorbents determined by inverse size-exclusion chromatography. *Journal of Chromatography A*, *883*(1-2), 39-54.

39. Carta, G., & Jungbauer, A. (2020). *Protein chromatography: process development and scale-up*. John Wiley & Sons. pp161-199.

40. Leweke, S., & von Lieres, E. (2018). Chromatography Analysis and Design Toolkit (CADET). *Computers & Chemical Engineering*, *113*, 274-294.

41. Hartmann, W. K., Saptharishi, N., Yang, X. Y., Mitra, G., & Soman, G. (2004). Characterization and analysis of thermal denaturation of antibodies by size exclusion high-performance liquid chromatography with quadruple detection. *Analytical Biochemistry*, *325*(2), 227-239.

42. Frey, D. D., Schweinheim, E., & Horvath, C. (1993). Effect of intraparticle convection on the chromatography of biomacromolecules. *Biotechnology Progress*, *9*(3), 273-284.

43. Satterfield, C. N. (1970). Mass transfer in heterogeneous catalysis. *MIT press.* Cambridge, MA.

44. Khanal, O., Kumar, V., Schlegel, F., & Lenhoff, A. M. (2020). Estimating and leveraging protein diffusion on ion-exchange resin surfaces. *Proceedings of the National Academy of Sciences*, 117(13), 7004-7010.

45. Wesselingh, J. A., & Bosma, J. C. (2001). Protein ion-exchange adsorption kinetics. *AIChE Journal*, *47*(7), 1571-1580.

46. Zydney, A. L., Harinarayan, C., & Van Reis, R. (2009). Modeling electrostatic exclusion effects during ion exchange chromatography of monoclonal antibodies. *Biotechnology and Bioengineering,* 102(4), 1131-1140.

47. Bhambure, R., Angelo, J. M., Gillespie, C. M., Phillips, M., Graalfs, H., & Lenhoff, A. M. (2017). Ionic strength-dependent changes in tentacular ion exchangers with variable ligand density. II. Functional properties. *Journal of Chromatography A,* 1506, 55-64.

48. DePhillips, P., & Lenhoff, A. M. (2001). Determinants of protein retention characteristics on cation-exchange adsorbents. *Journal of Chromatography A*, 933(1-2), 57-72.

Figure captions

Fig. 1. Elution peak shape for different systems with increasing loadings, approaching the saturation capacity. (A) Lysozyme on SP Sepharose FF, (B) mAb on Sepharose FF, (C) mAb on Fractogel SO_3^-, (D) lysozyme on Capto ImpRes SP, (E) cytochrome c on Fractogel SO_3^-, (F) lysozyme on Fractogel SO_3^-.

Fig. 2. (A) Breakthrough data for the mAb with changing IS on Fractogel SO_3^-. (B) Model simulation of a breakthrough curve with varying surface diffusivity (10^{-12} – 10^{-14} m^2s^{-1}). (C) Model simulation of breakthrough profiles for a mAb inside the column (along the length). (D) Model simulation of breakthrough profile for fixed B_{pp} but varying K_e. (E) Model simulation of breakthrough profile for varying B_{pp} but fixed K_e.

Fig. 3. Lysozyme on Capto SP ImpRes. (A) Breakthrough fits for model simulations. (B) Variation of K_e and B_{pp} with IS. (C) Variation of D_s with IS. (D) Comparison of gradient elution experiments and predictions. (E) Plot of calculated isotherm from model.

Fig. 4. (A) Breakthrough data fits using screening parameter calculated from Eq. 9. (B) Residual plot for different screening lengths (nm) for breakthrough data fits for varying IS. (C) and (D) Variations of K_e and B_{pp} with screening length (nm) for breakthrough data at different IS.

Fig. 5. Breakthrough profile predictions for the mAb at different flowrates. (A) 70 mM IS. (B) 100 mM IS.

Fig. 6. MAb on Fractogel SO_3^-. (A) Breakthrough data fits for model simulations at pH 5.5. (B - E) K_e, B_{pp}, D_s trends with varying IS. (F) D_s trend as a function of K_e at pH 5.5. (G - I) Plots of isotherms calculated from model for pH 5.5, 5.0 and 6.0.

Fig. 7. Prediction of elution profile for the mAb on Fractogel SO_3^-. (A) 50% load, 150 cm/h; (B) 75% load, 150 cm/h; (C) >100% load, 150 cm/h; (D) 75% load, 84 cm/h; (E) 50% load, 300 cm/h; (F) >100% load, 300 cm/h; (G) partial breakthrough at 90 mM IS; (H) full breakthrough at 60 mM IS; (I) full breakthrough at 80 mM IS.

Fig. 8. Universal fits of calibrated values of parameters for diffferent pH and IS for K_e and B_{pp} for mAb on Fractogel SO_3^- using Eq. (14) and (15).

Fig. 9. K_e and B_{pp} trends with IS for the mAb. (A-D) High (hi), standard (-), and low ligand-density variants of Fractogel SO_3^-. (E) and (F) SP Sepharose FF (SPFF), Toyopearl SP650M (TPS), Capto S (CPS) and Fractogel SO_3^- (-). (G) and (H) D_s variation with K_e for the mAb on different resins.

Figures 1-9

Click here to access/download;Figure;FiguresModelpaperV3.pptx

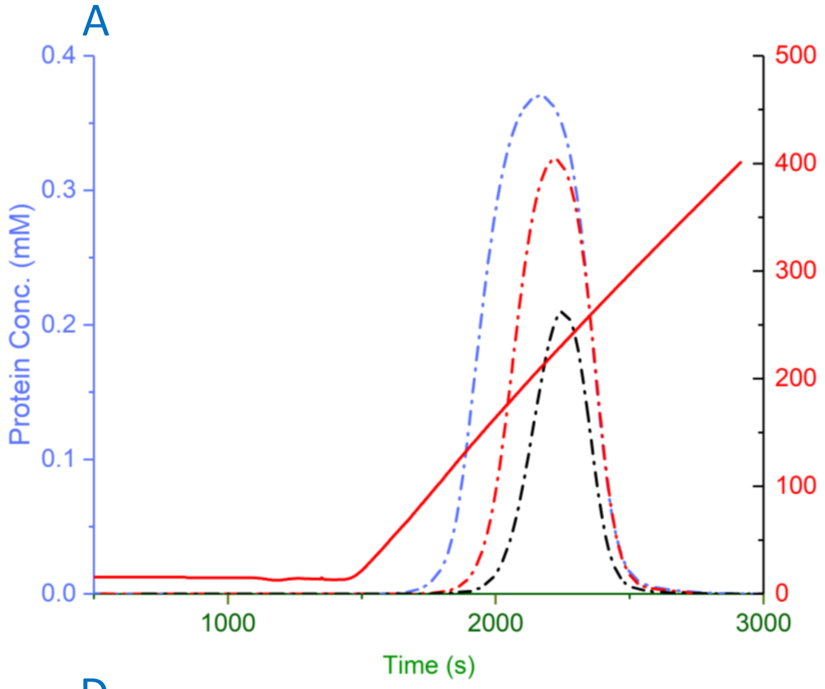

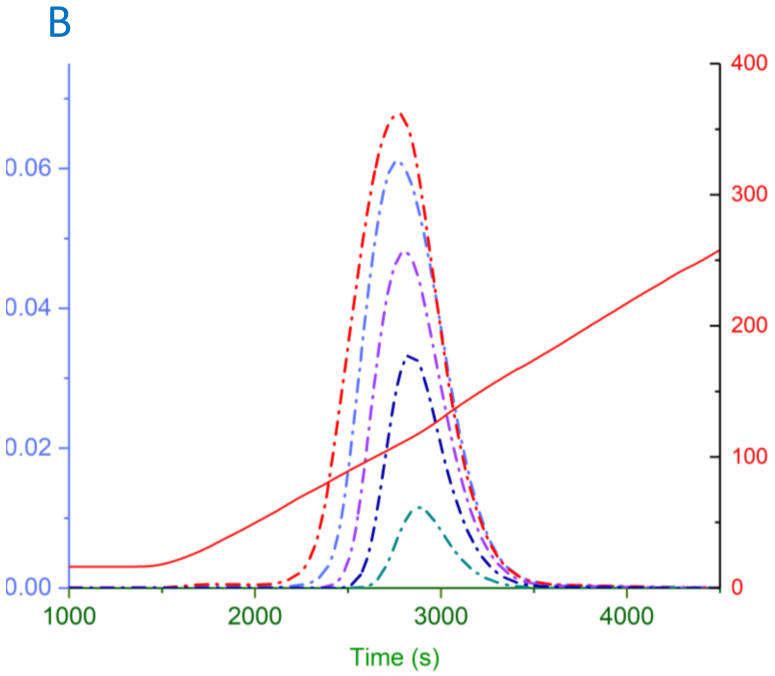

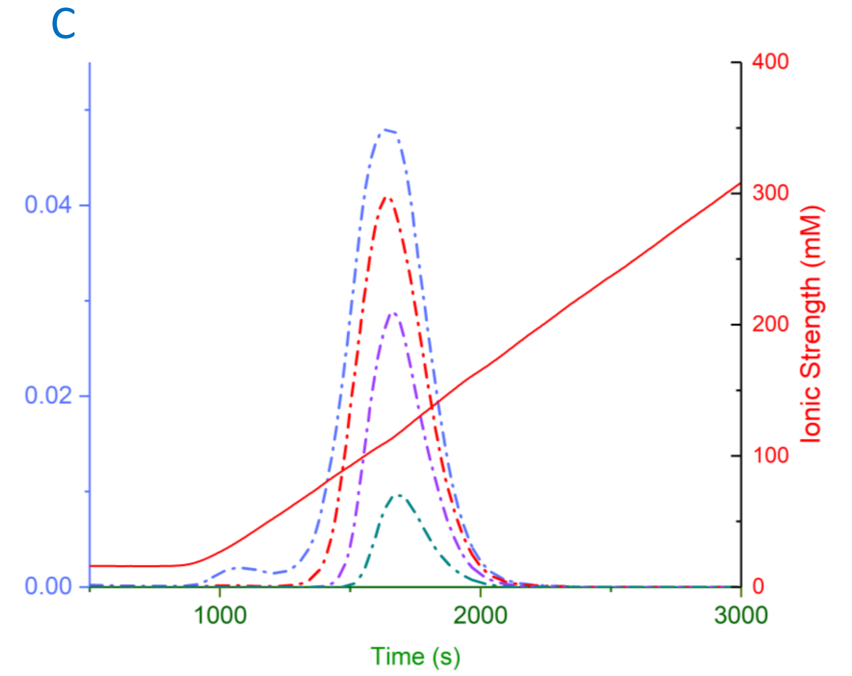

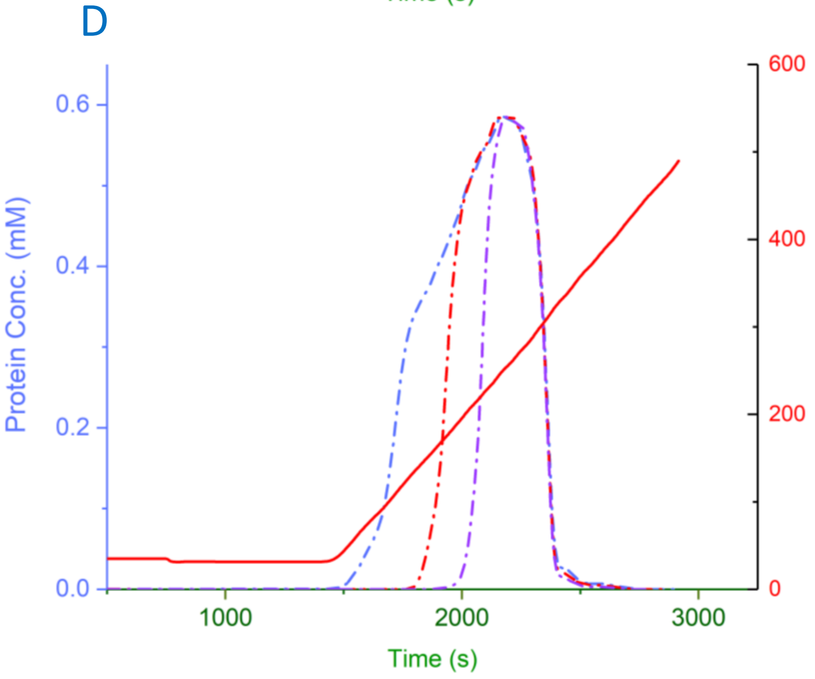

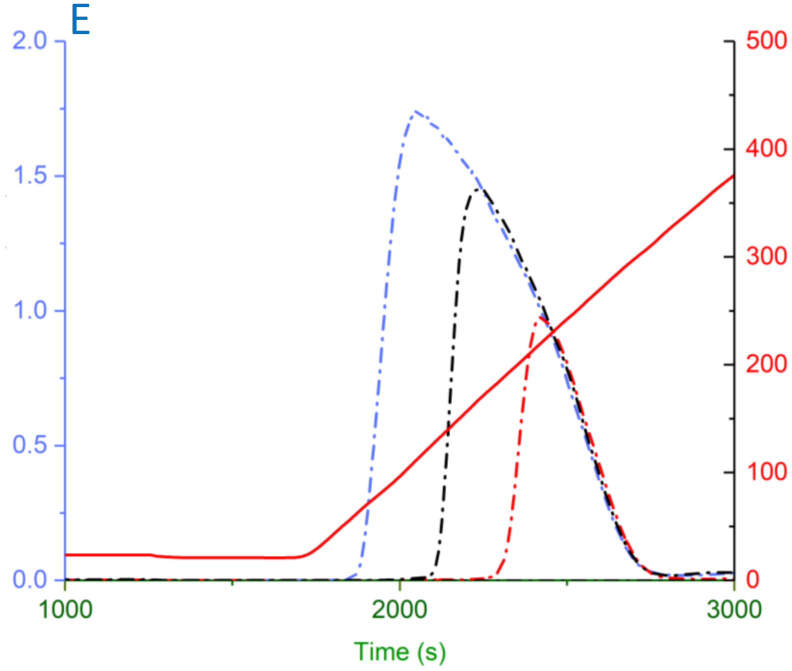

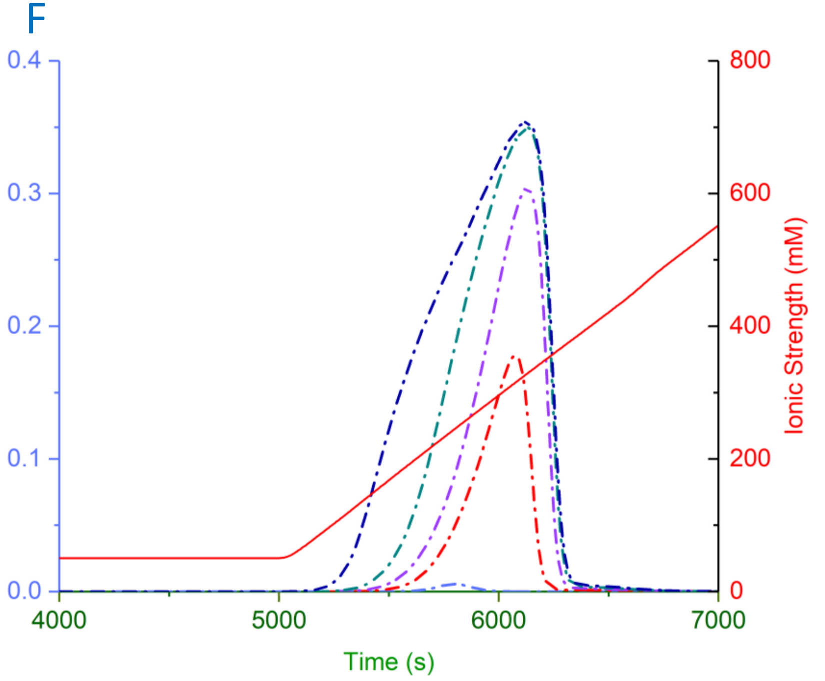

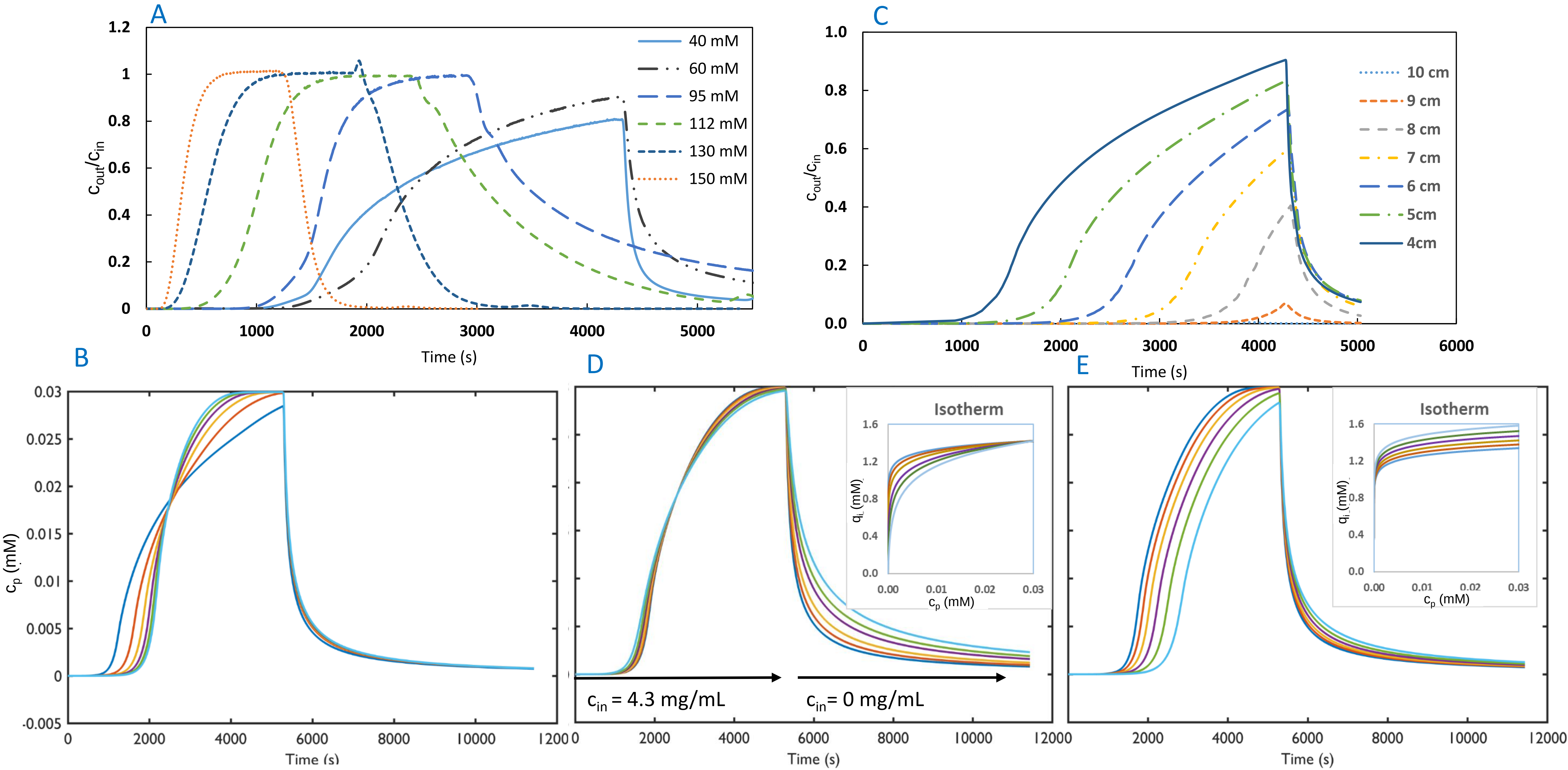
A
1.2
1
0.8
0.6
0.4
0.2
0
c_{out}/c_{in}
0
1000
2000
3000
4000
5000
Time (s)
40 mM
60 mM
95 mM
112 mM
130 mM
150 mM
C
1.0
0.8
0.6
0.4
0.2
0.0
c_{out}/c_{in}
0
1000
2000
3000
4000
5000
6000
Time (s)
10 cm
9 cm
8 cm
7 cm
6 cm
5cm
4cm
B
0.03
0.025
0.02
0.015
0.01
0.005
0
-0.005
c_p (mM)
0
2000
4000
6000
8000
10000
12000
Time (s)
D
0
2000
4000
6000
8000
10000
12000
Time (s)
c_{in} = 4.3 mg/mL
c_{in} = 0 mg/mL
Isotherm
1.6
1.2
0.8
0.4
0.0
q_i (mM)
0.00
0.01
0.02
0.03
c_p (mM)
E
0
2000
4000
6000
8000
10000
12000
Time (s)
Isotherm
1.6
1.2
0.8
0.4
0.0
q_i (mM)
0.00
0.01
0.02
0.03
c_p (mM)

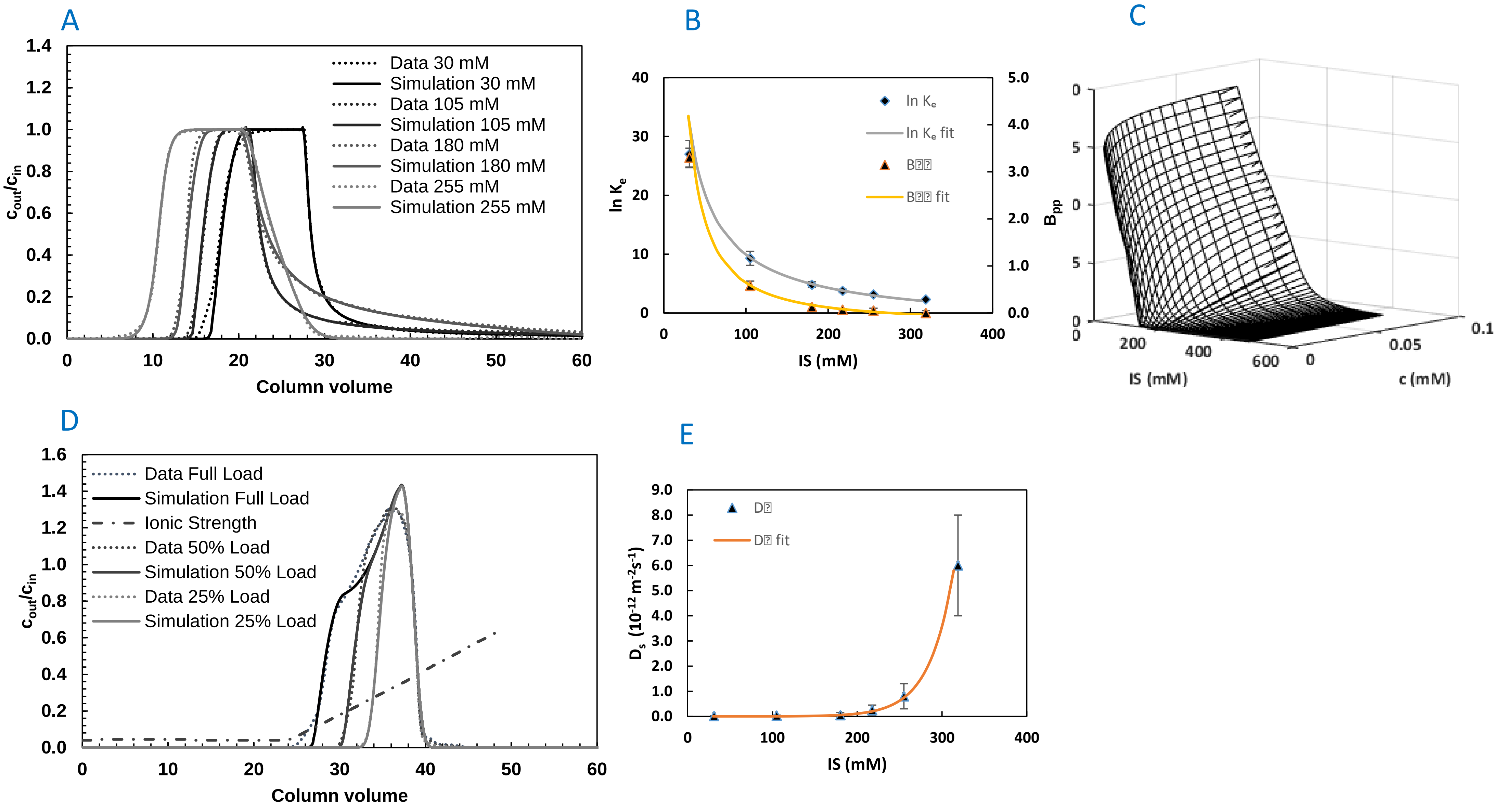
A
1.4
1.2
1.0
0.8
0.6
0.4
0.2
0.0
c_{out}/c_{in}
0
10
20
30
40
50
60
Column volume
Data 30 mM
Simulation 30 mM
Data 105 mM
Simulation 105 mM
Data 180 mM
Simulation 180 mM
Data 255 mM
Simulation 255 mM
B
40
30
20
10
0
ln K_e
5.0
4.0
3.0
2.0
1.0
0.0
0
100
200
300
400
IS (mM)
ln K_e
ln K_e fit
B□□
B□□ fit
C
0
5
0
5
0
B_{pp}
200
400
600
IS (mM)
0
0.05
0.1
c (mM)
D
1.6
1.4
1.2
1.0
0.8
0.6
0.4
0.2
0.0
c_{out}/c_{in}
0
10
20
30
40
50
60
Column volume
Data Full Load
Simulation Full Load
Ionic Strength
Data 50% Load
Simulation 50% Load
Data 25% Load
Simulation 25% Load
E
9.0
8.0
7.0
6.0
5.0
4.0
3.0
2.0
1.0
0.0
D_s (10^{-12} $m^{-2}s^{-1}$)
0
100
200
300
400
IS (mM)
D□
D□ fit

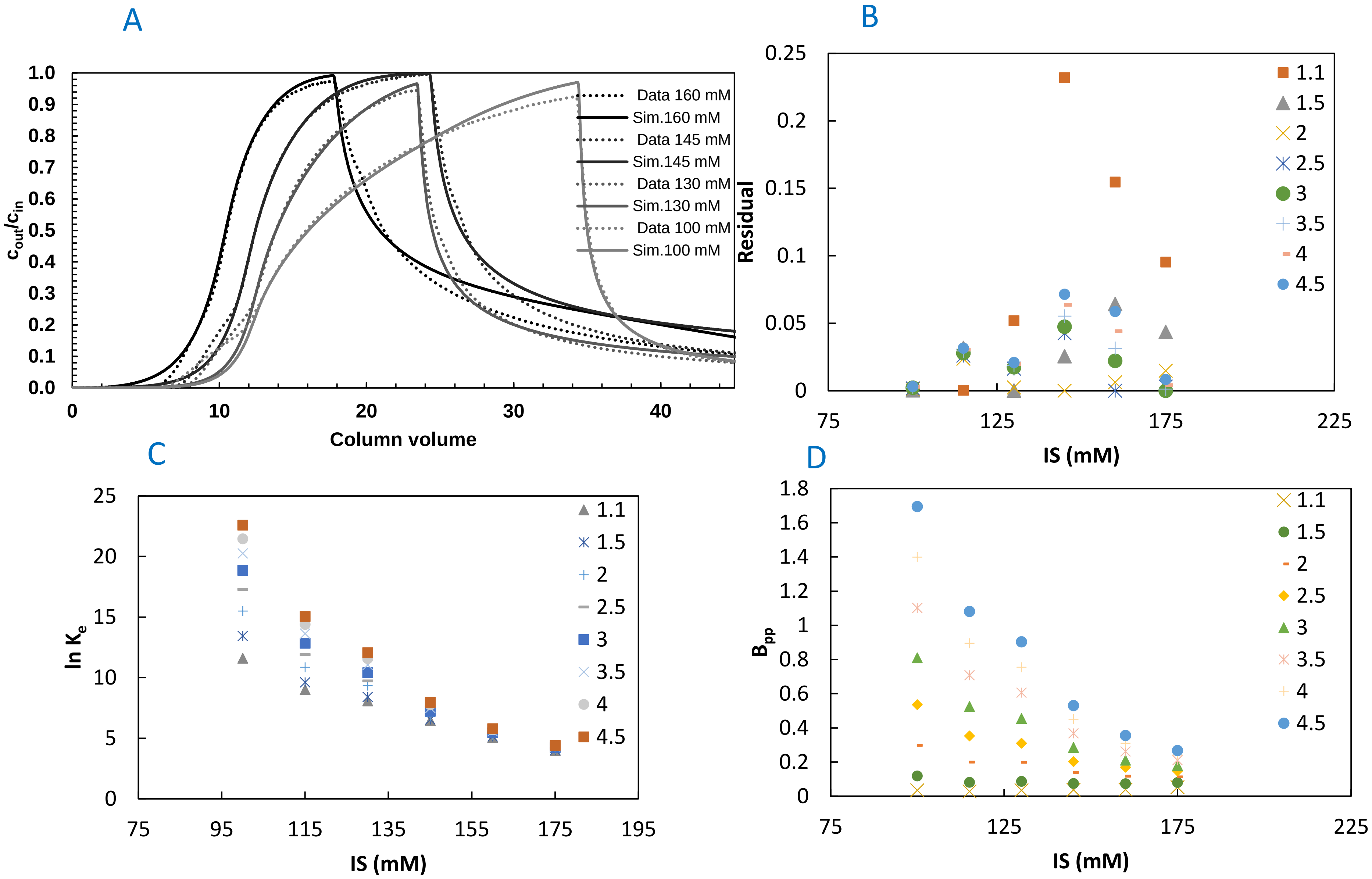
A
1.0
0.9
0.8
0.7
0.6
0.5
0.4
0.3
0.2
0.1
0.0
c_{out}/c_{in}
0
10
20
30
40
Column volume
Data 160 mM
Sim.160 mM
Data 145 mM
Sim.145 mM
Data 130 mM
Sim.130 mM
Data 100 mM
Sim.100 mM
B
0.25
0.2
0.15
0.1
0.05
0
Residual
75
125
175
225
IS (mM)
1.1
1.5
2
2.5
3
3.5
4
4.5
C
25
20
15
10
5
0
ln K_e
75
95
115
135
155
175
195
IS (mM)
1.1
1.5
2
2.5
3
3.5
4
4.5
D
1.8
1.6
1.4
1.2
1
0.8
0.6
0.4
0.2
0
B_{pp}
75
125
175
225
IS (mM)
1.1
1.5
2
2.5
3
3.5
4
4.5

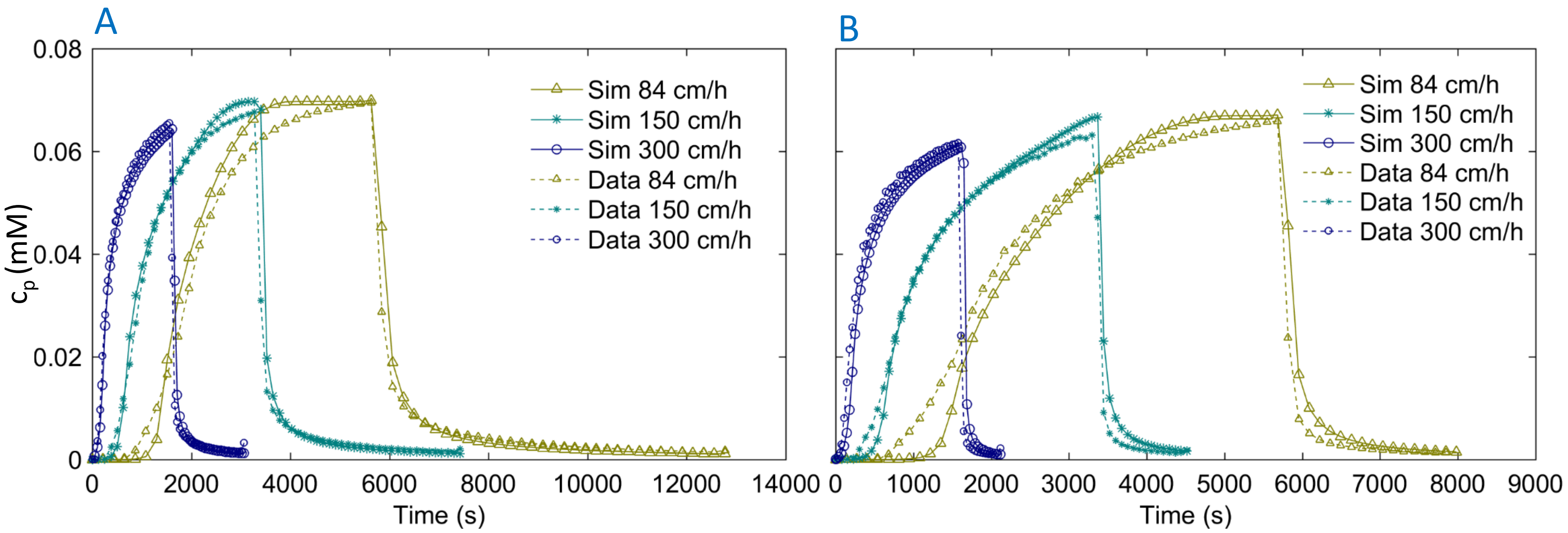
A
B
0.08
0.06
0.04
0.02
0
c_p (mM)
0
2000
4000
6000
8000
10000
12000
14000
0
1000
2000
3000
4000
5000
6000
7000
8000
9000
Time (s)
Time (s)
Sim 84 cm/h
Sim 150 cm/h
Sim 300 cm/h
Data 84 cm/h
Data 150 cm/h
Data 300 cm/h
Sim 84 cm/h
Sim 150 cm/h
Sim 300 cm/h
Data 84 cm/h
Data 150 cm/h
Data 300 cm/h

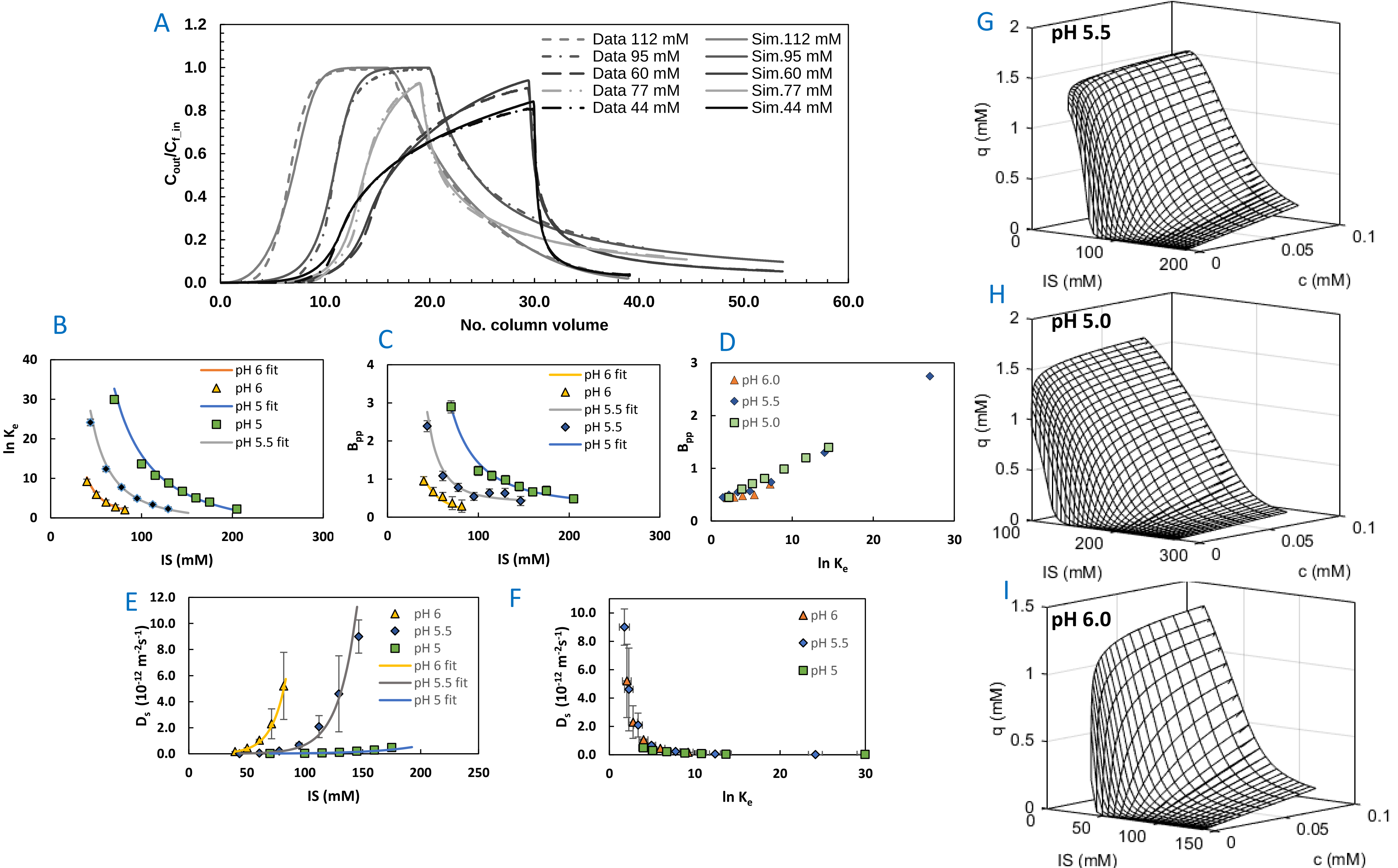
A
1.2
1.0
0.8
0.6
0.4
0.2
0.0
C_{out}/C_{f_in}
0.0
10.0
20.0
30.0
40.0
50.0
60.0
No. column volume
Data 112 mM
Data 95 mM
Data 60 mM
Data 77 mM
Data 44 mM
Sim.112 mM
Sim.95 mM
Sim.60 mM
Sim.77 mM
Sim.44 mM
B
40
30
20
10
0
$\ln K_e$
0
100
200
300
IS (mM)
pH 6 fit
pH 6
pH 5 fit
pH 5
pH 5.5 fit
C
4
3
2
1
0
B_{pp}
0
100
200
300
IS (mM)
pH 6 fit
pH 6
pH 5.5 fit
pH 5.5
pH 5 fit
D
3
2
1
0
B_{pp}
0
10
20
30
$\ln K_e$
pH 6.0
pH 5.5
pH 5.0
E
12.0
10.0
8.0
6.0
4.0
2.0
0.0
D_s (10^{-12} $m^{-2}s^{-1}$)
0
50
100
150
200
250
IS (mM)
pH 6
pH 5.5
pH 5
pH 6 fit
pH 5.5 fit
pH 5 fit
F
10.0
8.0
6.0
4.0
2.0
0.0
D_s (10^{-12} $m^{-2}s^{-1}$)
0
10
20
30
$\ln K_e$
pH 6
pH 5.5
pH 5
G
pH 5.5
2
1.5
1
0.5
0
q (mM)
0
100
200
IS (mM)
0
0.05
0.1
c (mM)
H
pH 5.0
2
1.5
1
0.5
0
q (mM)
100
200
300
IS (mM)
0
0.05
0.1
c (mM)
I
pH 6.0
1.5
1
0.5
0
q (mM)
0
50
100
150
IS (mM)
0
0.05
0.1
c (mM)

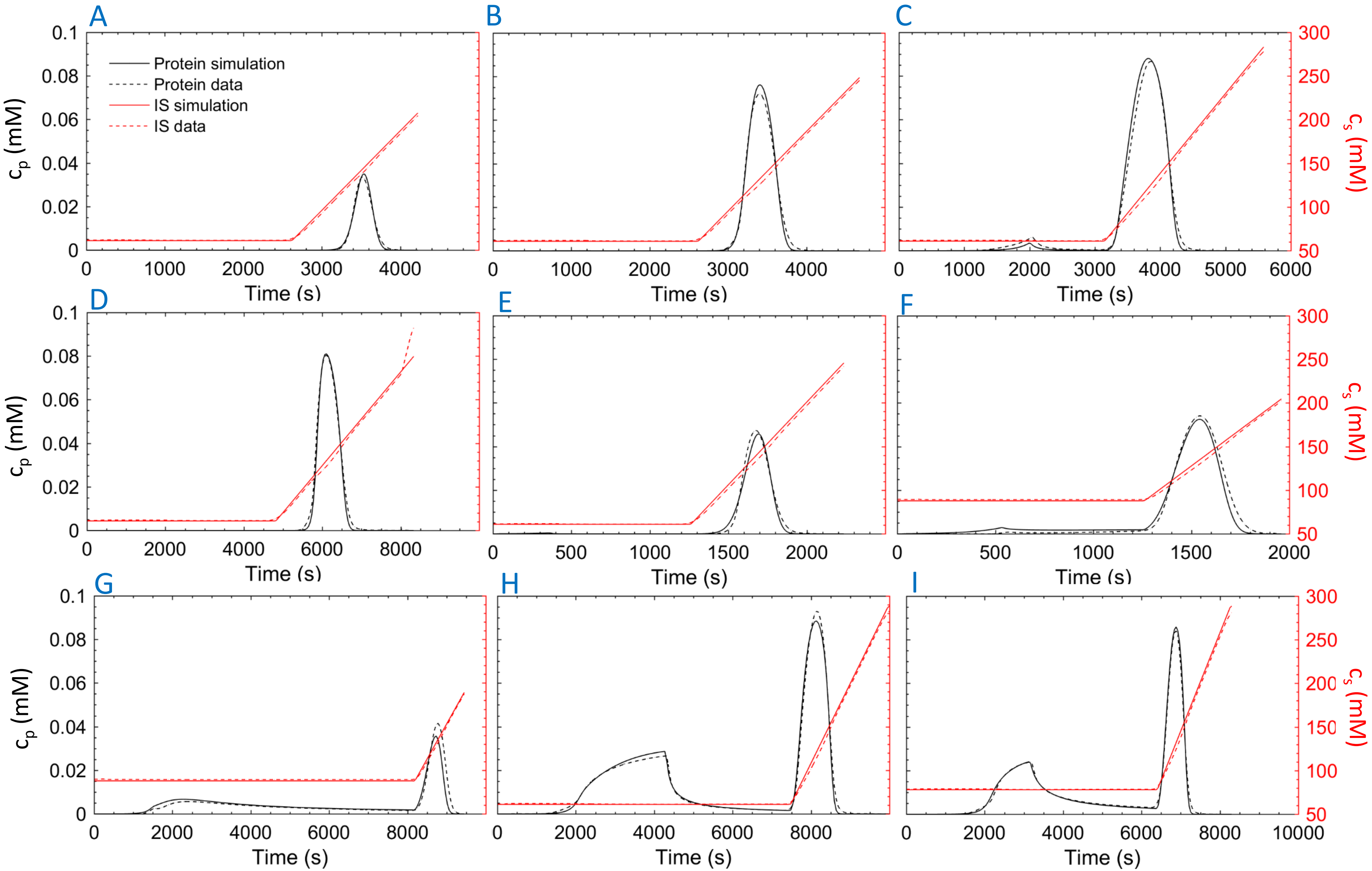
A
B
C
D
E
F
G
H
I
Protein simulation
Protein data
IS simulation
IS data
c_p (mM)
c_s (mM)
Time (s)
0.1
0.08
0.06
0.04
0.02
0
300
250
200
150
100
50
0
1000
2000
3000
4000
5000
6000
0
2000
4000
6000
8000
0
500
1000
1500
2000
10000

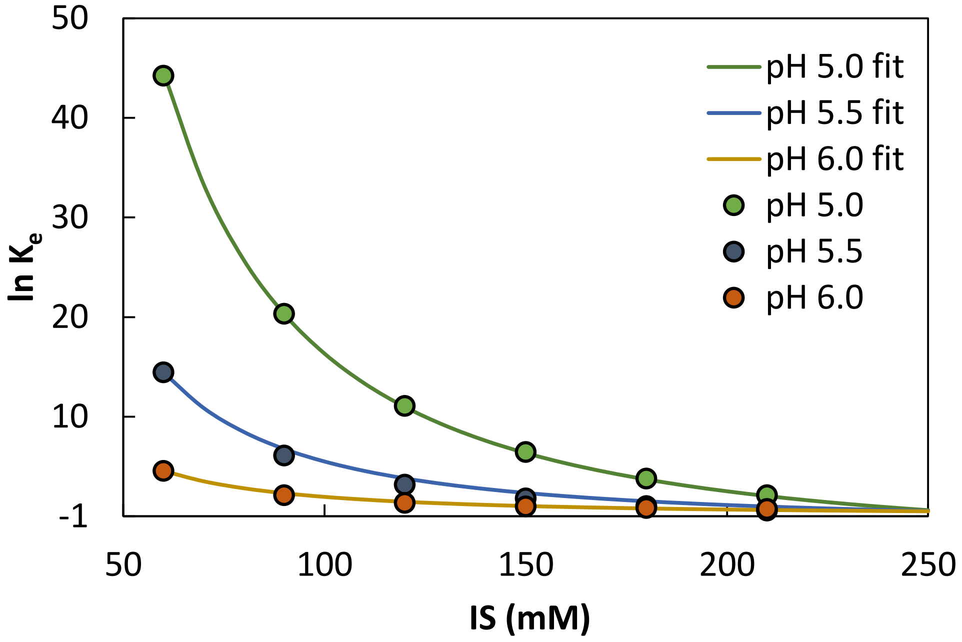

ln K$_e$
50
40
30
20
10
-1
50
100
150
200
250
IS (mM)
pH 5.0 fit
pH 5.5 fit
pH 6.0 fit
pH 5.0
pH 5.5
pH 6.0

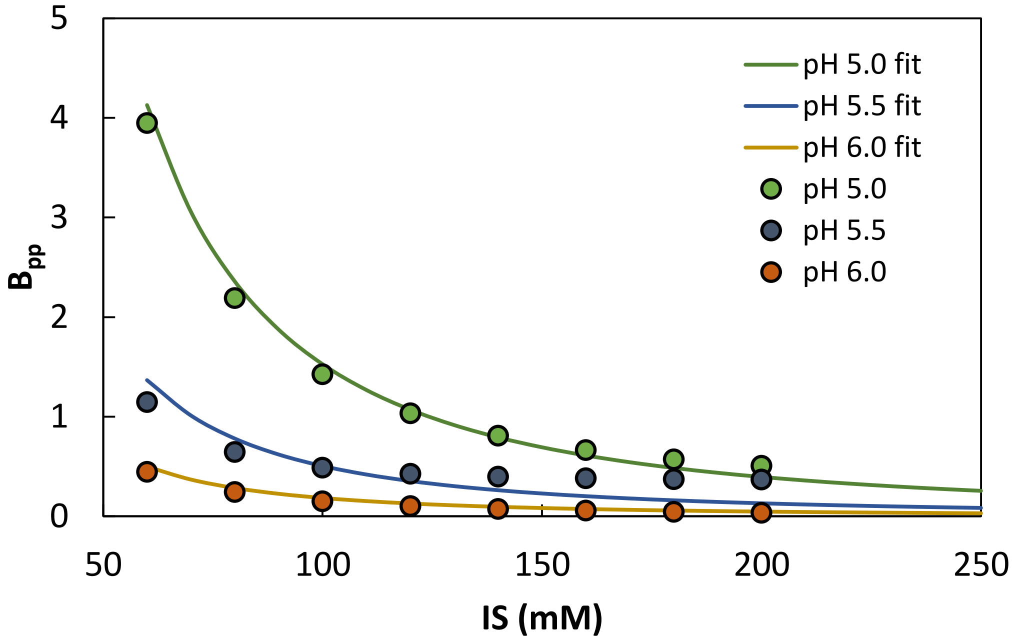

B$_{pp}$
5
4
3
2
1
0
50
100
150
200
250
IS (mM)
pH 5.0 fit
pH 5.5 fit
pH 6.0 fit
pH 5.0
pH 5.5
pH 6.0

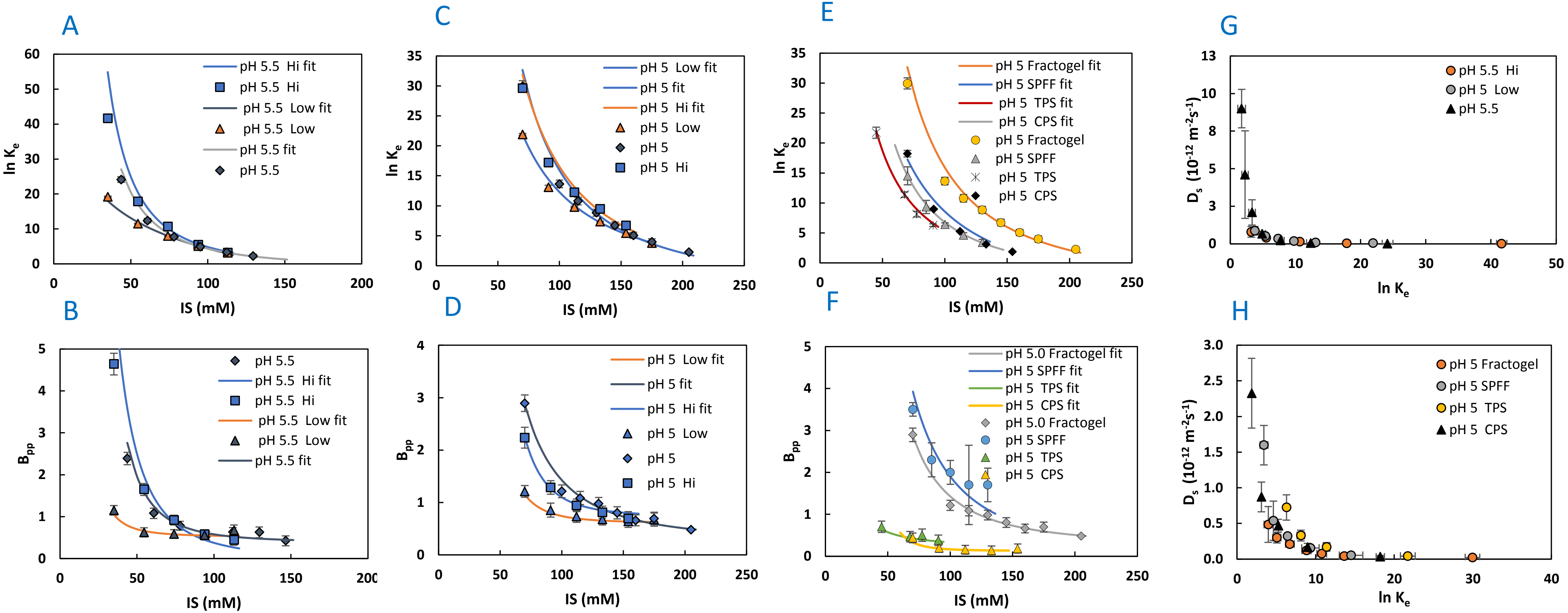
A
ln K$_e$
IS (mM)
pH 5.5 Hi fit
pH 5.5 Hi
pH 5.5 Low fit
pH 5.5 Low
pH 5.5 fit
pH 5.5
B
B$_{pp}$
IS (mM)
pH 5.5
pH 5.5 Hi fit
pH 5.5 Hi
pH 5.5 Low fit
pH 5.5 Low
pH 5.5 fit
C
ln K$_e$
IS (mM)
pH 5 Low fit
pH 5 fit
pH 5 Hi fit
pH 5 Low
pH 5
pH 5 Hi
D
B$_{pp}$
IS (mM)
pH 5 Low fit
pH 5 fit
pH 5 Hi fit
pH 5 Low
pH 5
pH 5 Hi
E
ln K$_e$
IS (mM)
pH 5 Fractogel fit
pH 5 SPFF fit
pH 5 TPS fit
pH 5 CPS fit
pH 5 Fractogel
pH 5 SPFF
pH 5 TPS
pH 5 CPS
F
B$_{pp}$
IS (mM)
pH 5.0 Fractogel fit
pH 5 SPFF fit
pH 5 TPS fit
pH 5 CPS fit
pH 5.0 Fractogel
pH 5 SPFF
pH 5 TPS
pH 5 CPS
G
D$_s$ (10^{-12} m^{-2}s^{-1})
ln K$_e$
pH 5.5 Hi
pH 5 Low
pH 5.5
H
D$_s$ (10^{-12} m^{-2}s^{-1})
ln K$_e$
pH 5 Fractogel
pH 5 SPFF
pH 5 TPS
pH 5 CPS

Electronic Supplementary Material (online publication only)

Click here to view linked References

Click here to access/download

Electronic Supplementary Material (online publication only)

Alldata_simulations.xlsx

The authors have no interests to declare.